We did not detect the association of Mal with PI(3)K-p85 in unstimulated neutrophils from healthy controls; however, we did observe this association in Btk-deficient neutrophils before stimulation with PMA (**Fig. 6d**). Moreover, confocal fluorescence microscopy showed targeting of the PI(3)K-p85–Mal complex to the membrane in the absence of Btk, whereas we observed the complex at the membrane after stimulation with PMA in the presence of Btk (**Fig. 6e**). In addition, most of the PI(3)K-p85 and Mal was present in the membrane fraction in neutrophils from patients with XLA (**Fig. 6f**). These data suggested that Btk in resting neutrophils was involved in confining Mal to the cytoplasm.

The mode of the Btk-Mal association

Btk phosphorylates Mal at Tyr86, Tyr106 and Tyr187, and the Btk-Mal interaction requires Pro125, Tyr86, Tyr106 and Tyr159 in Mal, whereas the critical site in Btk for this association remains unknown[21,22]. To clarify the region of Btk required for the cytoplasmic Btk-Mal association, we generated various Btk deletion mutants fused to histidine-tagged Hph-1 (**Fig. 7a**) and assessed their binding to Mal (**Fig. 7**). We incubated nickel bead–bound recombinant proteins with the cytoplasmic fraction of control neutrophils and evaluated the associations by immunoblot analysis with anti-Mal. Full-length Btk effectively bound to cytoplasmic Mal prepared from control neutrophils, but a control fusion of histidine-tagged Hph-1 and enhanced green fluorescent protein (eGFP) did not. Btk with deletion of the kinase domain almost completely lost the ability to interact with Mal, and Btk with deletion of the PH domain showed less binding to Mal. In contrast, recombinant proteins lacking the Tec homology domain, the Src homology 3 domain or the Src homology 2 domain had slightly greater capacity to associate with Mal (**Fig. 7b,d**). Other truncated Btk recombinant proteins without either the PH domain or kinase domain failed to bind to Mal (**Fig. 7c,d**), which suggested that both the PH domain and kinase domain are critical for the Btk-Mal interaction.

PTKs associate with Mal and regulate PI(3)K activation

The precise mechanism of PI(3)K activation triggered by membrane-associated Mal is largely unknown. As several PTKs were phosphorylated

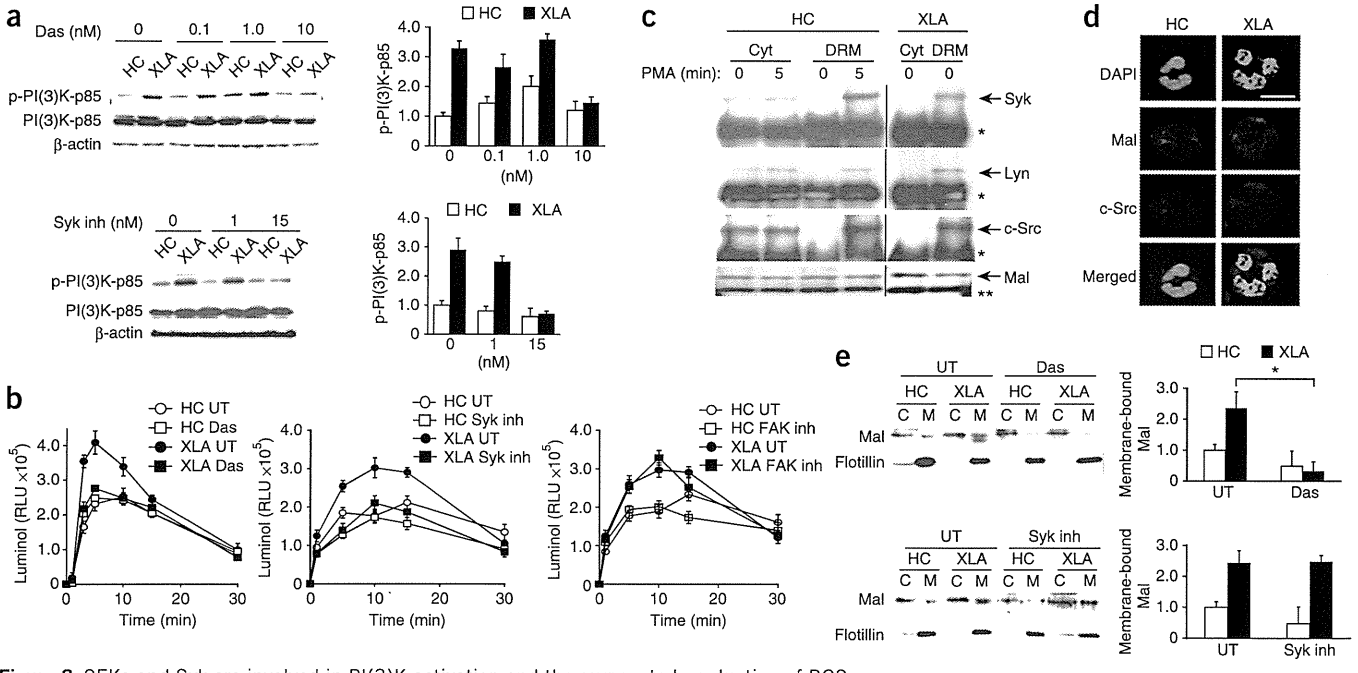

Figure 8 SFKs and Syk are involved in PI(3)K activation and the augmented production of ROS, whereas SFKs are involved in the membrane localization of Mal, in Btk-deficient neutrophils. (**a**) Immunoblot analysis (left of each pair) of total and phosphorylated PI(3)K-p85 in neutrophils from healthy controls and patients with XLA ($n = 4$ per group), treated with dasatinib (Das; at 10 nM, to inhibit the activity of c-Src, Lyn and Bcr-Abl but not FAK or Syk directly[36]) or a Syk inhibitor (Syk inh). Right (of each pair), densitometry of PI(3)K-p85 phosphorylated at Tyr508, presented as band intensity relative to that in untreated neutrophils from healthy controls, set as 1. (**b**) H_2O_2 production in neutrophils ($n = 4$ donors per group) left untreated (UT) or pretreated with dasatinib (10 nM), Syk inhibitor (15 nM) or FAK inhibitor (4 nM), and then stimulated with PMA, assessed by luminol assay and presented in relative light units (RLU). (**c**) Immunoassay of cytosolic fractions (Cyt) and detergent-resistant membrane fractions (DRM) of neutrophils from healthy controls and patients with XLA, left untreated (0) or treated for 5 min with PMA (5), followed by immunoprecipitation with anti-Mal and immunoblot analysis with anti-Syk, anti-Lyn, anti-c-Src or anti-Mal. *, immunoglobulin heavy chain; **, immunoglobulin light chain. (**d**) Confocal microscopy of neutrophils from healthy controls and patients with XLA ($n = 3$ per group), stained with anti-Mal (red) and anti-c-Src (blue) and counterstained with DAPI. Original magnification, ×600; scale bar, 10 μm. (**e**) Immunoblot analysis (left) of Mal in the cytoplasm (C) and membrane (M) of neutrophils from healthy controls and patients with XLA ($n = 5$ per group), left untreated or treated as in **a**. Right, quantification of results for Mal (left), presented relative to that of flotillin in the membrane fraction of neutrophils from healthy controls, set as 1. *$P = 0.0024$ (Student's *t*-test). (**f**) Immunoblot analysis of total Syk and Syk phosphorylated at Tyr524 and Tyr525 (top left) and of total c-Src and c-Src phosphorylated at Tyr416 (bottom left) in neutrophils from healthy controls and patients with XLA, left untreated or treated with dasatinib (top left) or Syk inhibitor (bottom left). Right, quantification of band intensity relative to that of β-actin in untreated neutrophils from healthy controls, set as 1. *$P = 0.013$ (Student's *t*-test). Data are from four (**a**) or five (**f**) independent experiments, are from one representative of four independent experiments (**c**) or are representative of four experiments (**b**,**e**) or three experiments (**c**; mean and s.d. in **a**,**b**,**e**,**f**).

in resting neutrophils from patients with XLA, we first used PTK inhibitors to investigate whether PTKs were involved in the PI(3)K activation. Inhibition of the activity of Src-family kinases (SFKs) by dasatinib (at a concentration of 10 nM)[36] led to normalized phosphorylation of PI(3)K-p85 in neutrophils derived from patients with XLA. Similarly, a Syk inhibitor (at a concentration of 15 nM)[37] but not a FAK inhibitor (at a concentration of 10 nM)[38] abrogated the hyperphosphorylation of PI(3)K (**Fig. 8a** and data not shown). The lower PI(3)K phosphorylation produced by dasatinib or the Syk inhibitor was accompanied by normalized production of ROS (**Fig. 8b**), which indicated that SFKs and Syk were involved in the augmented production of ROS in neutrophils from patients with XLA.

The findings noted above prompted us to determine whether the activated PTKs associated with Mal. SFKs are recruited to lipid rafts when activated for the assembly of signal components[39,40]. Coprecipitation assays showed that Lyn, c-Src and Syk interacted with Mal at the rafts of Btk-deficient neutrophils before stimulation (**Fig. 8c**). We also observed the colocalization of Mal and c-Src at the membrane by confocal fluorescence microscopy (**Fig. 8d**). We observed the interaction at the rafts of control neutrophils only after stimulation with PMA (**Fig. 8c** and **Supplementary Fig. 6**).

SFKs are cytoplasmic kinases and are anchored to the plasma membrane through myristoylation and palmitoylation[39,40]. Coprecipitation assays showed that Lyn, c-Src and Syk were associated with Mal in the cytosol of neutrophils from healthy controls but not in Btk-deficient neutrophils (**Fig. 8c**). We also confirmed by immunofluorescence staining the presence of c-Src associated with Mal in the cytoplasm but not in the membrane of normal resting neutrophils (**Fig. 8d**).

We next studied whether the membrane localization of Mal was regulated by SFKs or by Syk. The localization of Mal to the membrane in Btk-deficient neutrophils was diminished to normal amounts in cells treated with dasatinib but not those treated with the Syk inhibitor (**Fig. 8e**), which suggested that kinase activity of SFKs was required for membrane recruitment or maintenance of membrane-anchoring of Mal. Treatment of neutrophils from patients with XLA with dasatinib resulted in less baseline Syk phosphorylation, whereas incubation with the Syk inhibitor did not abrogate the hyperphosphorylation of c-Src (**Fig. 8f**), which indicated that Syk was downstream of SFKs in the steady-state signaling cascade of Btk-deficient neutrophils.

Collectively, the data reported above indicated that at least some PTKs associated with Mal together with Btk in the cytoplasm; in the absence of Btk, SFKs and Mal translocated to the membrane. The membrane-recruited PTKs formed a complex with and phosphorylated PI(3)K-p85 (**Supplementary Fig. 7**). It is still unclear which neutrophil SFK contributes to PI(3)K activation. Our findings may indicate that c-Src (or other SFKs) but not Lyn is (are) directly involved in the PI(3)K activation in Btk-deficient neutrophils; however, the possibility of an indirect contribution of Lyn to the phosphorylation of PI(3)K-p85 cannot be excluded solely by the inhibitor assay.

DISCUSSION

So far, most data have posited Btk as an essential molecule in innate immune responses[12–15,23,25]. Here we have shown that Btk is a negative regulator of signal transduction that leads to activation of NADPH oxidase and a molecule that prevents excessive neutrophil responses. Neutropenia in patients with XLA is usually induced by infection and is observed less often after immunoglobulin supplementation. This phenomenon can most probably be explained by ROS-mediated apoptosis of neutrophils triggered by the engagement of innate receptors and not by abnormal myeloid differentiation.

Our study suggested that Btk serves as a cytosolic component that interacts with Mal to prevent its translocation to the membrane and its interactions with PI(3)K until the appropriate stimulation is received. Both the PH and kinase domains of Btk were necessary for association with cytoplasmic Mal and were important for proper and coordinated initiation of the TLR and TNF receptor responses in human neutrophils. A similar mode of interaction has been demonstrated for the association of Btk with the cell-surface death receptor Fas (CD95) in B cells. Btk associates with Fas via its PH and kinase domains and prevents the interaction of Fas with the Fas-associated death domain and thus serves as a negative regulator of the Fas death-inducing signaling complex[41]. Notably, Btk serves as a negative regulator of apoptosis in both signaling systems.

SFKs were also involved in the baseline activation of PI(3)K in Btk-deficient neutrophils. We detected the association of c-Src, Lyn and Syk with Mal in the membrane raft in the absence of Btk. In addition, localization of Mal to the membrane in Btk-defective neutrophils was dependent on SFKs. These findings may indicate that SFKs serve as a substitute for the function of Btk in guiding the localization of Mal, albeit in an unregulated way. In neutrophils from control subjects, SFKs and Mal were associated in the cytoplasm and localized to the raft after stimulation. The mode of the SFK-Mal interaction remains unclear; however, we speculate that the kinase domain is involved, as SFKs lack a PH domain and the kinase domains of SFKs and Btk share 40–45% homology. Precise mapping of the Mal-binding site in the Btk kinase domain would help to clarify the SFK-Mal association site. Notably, neutrophils had more abundant expression of Mal than did monocytes (data not shown). Our data suggest that Mal is a critical coordinator of the priming signal and that its localization is tightly controlled by Btk.

Limited data indicate a role for PTKs in the production of ROS in neutrophils, particularly in humans. Lyn is reported to be a signaling component of the immunoglobulin receptors FcγRI and FcγRII or the receptor for the hematopoietic cytokine G-CSF, as well as an activator of PI(3)K[30,42], but is also noted for its ability to negatively regulate myeloid-cell signaling through phosphorylation of inhibitory receptors and recruitment of phosphatases[29]. Lyn-deficient neutrophils produce less ROS than Lyn-sufficient neutrophils do after stimulation with G-CSF[30] but show an enhanced respiratory burst after integrin-mediated signaling[29,31]. ROS responses triggered by *Aspergillus* species are totally dependent on Syk in mouse neutrophils[43]. The phosphorylation at different regulatory sites in Lyn versus c-Src in Btk-deficient neutrophils is notable. However, overall, PTKs in unstimulated neutrophils from patients with XLA seem to function as positive signal regulators. These data, along with our observations, suggest a potential contribution of SFKs and Syk to the early phase of NADPH oxidase activation in human neutrophils.

Activation of TFKs occurs downstream of SFKs in signaling pathways[40]. However, in neutrophils, Btk regulates baseline SFK activation. There are several possible mechanisms to explain how defective Btk is connected to SFK activation. We first speculated that Btk controls SFKs through the activation of negative SFK regulators. We investigated the Src kinase Csk and its regulatory molecule Cbp[44], but found no difference in the expression, localization or phosphorylation of Csk or Cbp (data not shown). As a second possible mechanism, SFKs but not TFKs may have been activated to compensate for Btk function in neutrophils. It is noteworthy that Btk regulates PtdIns(4,5)P_2 synthesis, acting as a shuttle to bring type I phosphatidylinositol-4-phosphate 5-kinases to the plasma membrane in B cells[45]. Although the role of Btk in PtdIns(4,5)P_2 production in human neutrophils has not been addressed, the generation of PtdIns(4,5)P_2 is a critical

step in the activation of NADPH oxidase. SFKs may have directly or indirectly served as a substitute for the function of Btk in neutrophils from patients with XLA. Finally, the cytoplasmic association of SFKs with Mal but without Btk may have resulted in SFK activation and Lyn inhibition. The phosphorylation of SFKs and subsequent modification of Mal by SFKs may have led to the translocation of Mal in the absence of Btk.

Neutrophils from patients with XLA show excessive production of ROS, but neutrophils from mice with X-linked immunodeficiency show poor ROS induction[15]. One possibility that could explain this discrepancy is the difference between mice and humans in the involvement of Btk in the NADPH oxidase pathway. Another possibility is the difference in the contributions of various members of the PI(3)K family to neutrophil activation. The primed production of ROS requires sequential activation of PI(3)Kγ and PI(3)Kδ in humans, whereas the production of ROS is largely dependent on PI(3)Kγ alone in mice[46]. A third possibility is differences in the methods of neutrophil collection from mice and in our study. Neutrophils collected from the peritoneum after treatment with thioglycolate broth may have been stimulated by that treatment[15]. The production of ROS was not augmented or compromised in neutrophils from patients with XLA in one study[26]. That may also have resulted from a relatively harsh isolation technique of hypotonic shock or from non–endotoxin-free conditions (for example, lipopolysaccharide in FBS) at any point of the experiment.

In this study, we have reported that Btk serves as a critical gatekeeper of neutrophil response. Our study suggests that the regulation of neutrophil activation and apoptosis in various human diseases could be achieved by manipulation of Btk. Future studies should explore the role of Btk in controlling the production of ROS and apoptosis of basophils, mast cells and eosinophils. Finally, ROS-mediated induction of apoptosis after suboptimal or optimal stimuli may be worth investigating in immature and precursor cells of the immune reponse to determine the role of Btk in their survival, proliferation and differentiation.

METHODS

Methods and any associated references are available in the online version of the paper at http://www.nature.com/natureimmunology/.

Note: Supplementary information is available on the Nature Immunology website.

ACKNOWLEDGMENTS

We thank E. Tsitsikov, E. Rachlin, K. Imai and J. Yata for discussions; all patients who participated in this study; S. Goo Rhee (Ewha Womans University) for antibody to Prx1 phosphorylated at Tyr194; and J.A. Lindquist (Otto-von-Guericke University) for antibody to Cbp (PAG) phosphorylated at Tyr317. Supported by the Ministry of Health, Labour and Welfare of Japan (H. Kane, S.N. and T.M.), the Ministry of Education, Culture, Sports, Science and Technology of Japan (S.M. and T.M.) and by the National Research Foundation of Korea (National Creative Research Initiatives grant to S.-K.L.).

AUTHOR CONTRIBUTIONS

F.H. did experiments; E.-S.K. and S.-K.L. contributed to protein-delivery experiments and provided some technical support; H. Kano and H. Kane made suggestions on data analysis and interpretation; S.N. and S.M. provided advice on project planning and data interpretation; M.T. provided advice on project plan and edited the manuscript; T.M. directed the project, designed research and wrote the manuscript; and all authors reviewed and approved the manuscript.

COMPETING FINANCIAL INTERESTS

The authors declare no competing financial interests.

Published online at http://www.nature.com/natureimmunology/.
Reprints and permissions information is available online at http://www.nature.com/reprints/index.html.

1. Flannagan, R.S., Cosio, G. & Grinstein, S. Antimicrobial mechanisms of phagocytes and bacterial evasion strategies. *Nat. Rev. Microbiol.* **7**, 355–366 (2009).
2. Nauseef, W.M. How human neutrophils kill and degrade microbes: an integrated view. *Immunol. Rev.* **219**, 88–102 (2007).
3. Lambeth, J.D. NOX enzymes and the biology of reactive oxygen. *Nat. Rev. Immunol.* **4**, 181–189 (2004).
4. Babior, B.M. NADPH oxidase. *Curr. Opin. Immunol.* **16**, 42–47 (2004).
5. Sumimoto, H. Structure, regulation and evolution of Nox-family NADPH oxidases that produce reactive oxygen species. *FEBS J.* **275**, 3249–3277 (2008).
6. Fang, F.C. Antimicrobial reactive oxygen and nitrogen species: concepts and controversies. *Nat. Rev. Microbiol.* **2**, 820–832 (2004).
7. Singh, A., Zarember, K.A., Kuhns, D.B. & Gallin, J.I. Impaired priming and activation of the neutrophil NADPH oxidase in patients with IRAK4 or NEMO deficiency. *J. Immunol.* **182**, 6410–6417 (2009).
8. Woollard, K.J. & Geissmann, F. Monocytes in atherosclerosis: subsets and functions. *Nat. Rev. Cardiol.* **7**, 77–86 (2009).
9. Finkel, T. Radical medicine: treating ageing to cure disease. *Nat. Rev. Mol. Cell Biol.* **6**, 971–976 (2005).
10. Conley, M.E. *et al.* Genetic analysis of patients with defects in early B-cell development. *Immunol. Rev.* **203**, 216–234 (2005).
11. Winkelstein, J.A. *et al.* X-linked agammaglobulinemia: report on a United States registry of 201 patients. *Medicine (Baltimore)* **85**, 193–202 (2006).
12. Mohamed, A.J. *et al.* Bruton's tyrosine kinase (Btk): function, regulation, and transformation with special emphasis on the PH domain. *Immunol. Rev.* **228**, 58–73 (2009).
13. Gray, P. *et al.* MyD88 adapter-like (Mal) is phosphorylated by Bruton's tyrosine kinase during TLR2 and TLR4 signal transduction. *J. Biol. Chem.* **281**, 10489–10495 (2006).
14. Doyle, S.L., Jefferies, C.A., Feighery, C. & O'Neill, L.A. Signaling by Toll-like receptors 8 and 9 requires Bruton's tyrosine kinase. *J. Biol. Chem.* **282**, 36953–36960 (2007).
15. Mangla, A. *et al.* Pleiotropic consequences of Bruton tyrosine kinase deficiency in myeloid lineages lead to poor inflammatory responses. *Blood* **104**, 1191–1197 (2004).
16. Fiedler, K. *et al.* Neutrophil development and function critically depend on Bruton tyrosine kinase in a mouse model of X-linked agammaglobulinemia. *Blood* **117**, 1329–1339 (2011).
17. Conley, M.E. *et al.* Primary B cell immunodeficiencies: comparisons and contrasts. *Annu. Rev. Immunol.* **27**, 199–227 (2009).
18. Kerner, J.D. *et al.* Impaired expansion of mouse B cell progenitors lacking Btk. *Immunity* **3**, 301–312 (1995).
19. Khan, W.N. *et al.* Defective B cell development and function in Btk-deficient mice. *Immunity* **3**, 283–299 (1995).
20. O'Neill, L.A.J. & Bowie, A.G. The family of five: TIR-domain-containing adaptors in Toll-like receptor signalling. *Nat. Rev. Immunol.* **7**, 353–364 (2007).
21. Piao, W. *et al.* Tyrosine phosphorylation of MyD88 adapter-like (Mal) is critical for signal transduction and blocked in endotoxin tolerance. *J. Biol. Chem.* **283**, 3109–3119 (2008).
22. Jenkins, K.A. & Mansell, A. TIR-containing adaptors in Toll-like receptor signalling. *Cytokine* **49**, 237–244 (2010).
23. Taneichi, H. *et al.* Toll-like receptor signaling is impaired in dendritic cells from patients with X-linked agammaglobulinemia. *Clin. Immunol.* **126**, 148–154 (2008).
24. Pérez de Diego, R. *et al.* Bruton's tyrosine kinase is not essential for LPS-induced activation of human monocytes. *J. Allergy Clin. Immunol.* **117**, 1462–1469 (2006).
25. Horwood, N.J. *et al.* Bruton's tyrosine kinase is required for TLR2 and TLR4-induced TNF, but not IL-6, production. *J. Immunol.* **176**, 3635–3641 (2006).
26. Marron, T.U., Rohr, K., Martinez-Gallo, M., Yu, J. & Cunningham-Rundles, C. TLR signaling and effector functions are intact in XLA neutrophils. *Clin. Immunol.* **137**, 74–80 (2010).
27. Honda, F. *et al.* Transducible form of p47phox and p67phox compensate for defective NADPH oxidase activity in neutrophils of patients with chronic granulomatous disease. *Biochem. Biophys. Res. Commun.* **417**, 162–168 (2012).
28. Dang, P.M. *et al.* A specific p47phox -serine phosphorylated by convergent MAPKs mediates neutrophil NADPH oxidase priming at inflammatory sites. *J. Clin. Invest.* **116**, 2033–2043 (2006).
29. Scapini, P., Pereira, S., Zhang, H. & Lowell, C.A. Multiple roles of Lyn kinase in myeloid cell signaling and function. *Immunol. Rev.* **228**, 23–40 (2009).
30. Zhu, Q.S. *et al.* G-CSF induced reactive oxygen species involves Lyn-PI3-kinase-Akt and contributes to myeloid cell growth. *Blood* **107**, 1847–1856 (2006).
31. Pereira, S. & Lowell, C. The Lyn tyrosine kinase negatively regulates neutrophil integrin signaling. *J. Immunol.* **171**, 1319–1327 (2003).
32. Vlahos, C.J., Matter, W.F., Hui, K.Y. & Brown, R.F. A specific inhibitor of phosphatidylinositol 3-kinase, 2-(4-morpholinyl)-8-phenyl-4H–1-benzopyran-4-one (LY294002). *J. Biol. Chem.* **269**, 5241–5248 (1994).
33. Sadhu, C., Masinovsky, B., Dick, K., Sowell, C.G. & Staunton, D.E. Essential role of phosphoinositide 3-kinase δ in neutrophil directional movement. *J. Immunol.* **170**, 2647–2654 (2003).
34. Morris, A.C. *et al.* C5a-mediated neutrophil dysfunction is RhoA-dependent and predicts infection in critically ill patients. *Blood* **117**, 5178–5188 (2011).
35. Santos-Sierra, S. *et al.* Mal connects TLR2 to PI3Kinase activation and phagocyte polarization. *EMBO J.* **28**, 2018–2027 (2009).

36. Nam, S. *et al.* Action of the Src family kinase inhibitor, dasatinib (BMS-354825), on human prostate cancer cells. *Cancer Res.* **65**, 9185–9189 (2005).
37. Lai, J.Y. *et al.* Potent small molecule inhibitors of spleen tyrosine kinase (Syk). *Bioorg. Med. Chem. Lett.* **13**, 3111–3114 (2003).
38. Slack-Davis, J.K. *et al.* Cellular characterization of a novel focal adhesion kinase inhibitor. *J. Biol. Chem.* **282**, 14845–14852 (2007).
39. Korade-Mirnics, Z. & Corey, S.J. Src kinase-mediated signaling in leukocytes. *J. Leukoc. Biol.* **68**, 603–613 (2000).
40. Bradshaw, J.M. The Src, Syk, and Tec family kinases: distinct types of molecular switches. *Cell. Signal.* **22**, 1175–1184 (2010).
41. Vassilev, A., Ozer, Z., Navara, C., Mahajan, S. & Uckun, F.M. Bruton's tyrosine kinase as an inhibitor of the Fas/CD95 death-inducing signaling complex. *J. Biol. Chem.* **274**, 1646–1656 (1999).
42. Wang, A.V., Scholl, P.R. & Geha, R.S. Physical and functional association of the high affinity immunoglobulin G receptor (FcγRI) with the kinases Hck and Lyn. *J. Exp. Med.* **180**, 1165–1170 (1994).
43. Boyle, K.B. *et al.* Class IA phosphoinositide 3-kinase β and δ regulate neutrophil oxidase activation in response to *Aspergillus fumigatus* hyphae. *J. Immunol.* **186**, 2978–2989 (2011).
44. Kawabuchi, M. *et al.* Transmembrane phosphoprotein Cbp regulates the activities of Src-family tyrosine kinases. *Nature* **404**, 999–1003 (2000).
45. Saito, K. *et al.* BTK regulates PtdIns-4,5–P2 synthesis: importance for calcium signaling and PI3K activity. *Immunity* **19**, 669–678 (2003).
46. Condliffe, A.M. *et al.* Sequential activation of class IB and class IA PI3K is important for the primed respiratory burst of human but not murine neutrophils. *Blood* **106**, 1432–1440 (2005).
47. Uckun, F.M. *et al.* Anti-breast cancer activity of LFM-A13, a potent inhibitor of Polo-like kinase (PLK). *Bioorg. Med. Chem.* **15**, 800–814 (2007).
48. Mahajan, S. *et al.* Rational design and synthesis of a novel anti-leukemic agent targeting Bruton's tyrosine kinase (BTK), LFM-A13 [alpha-cyano-β-hydroxy-β-methyl-N-(2,5-dibromophenyl)propenamide]. *J. Biol. Chem.* **274**, 9587–9599 (1999).

ONLINE METHODS

Reagents and antibodies. The following reagents were used: lipopolysaccharide derived from *Escherichia coli* or *Pseudomonas aeruginosa*, fMLP, PMA, DHR123, luminol, N-acetyl cysteine, aprotinin, leupeptin, pepstatin and phenylmethyl sulfonyl fluoride (all from Sigma-Aldrich); recombinant human TNF (R&D Systems); Pam_3CSK_4, LFM-A13, LFM-A11, Syk inhibitor, FAK inhibitor and Ly294002 (all from Calbiochem); and dasatinib, IC87114 and AS-605240 (all from Biovision). Oligodeoxynucleotide CpG-A (5′-GGT GCATCGATGCAGGGGGG-3′) was from Operon Biotechnologies.

The antibodies used were as follows: goat polyclonal antibody to PI(3)K-p85α phosphorylated at Tyr508 (sc-12929), Hck phosphorylated at Tyr411 (sc-12928), rabbit polyclonal antibody to Hck (N-30), anti-PTEN (FL-403), anti-PTP-PEST (H130), anti-FAK (A-17), anti-Vav (C-14), anti-Syk (C-20), anti-SHP2 (C-18) and anti-SHP 1 (C-19), as well as mouse monoclonal antibody (mAb) to $p47^{phox}$ (D-10), $p40^{phox}$ (D-8) or $p22^{phox}$ (CS-9; all from Santa Cruz). Rabbit polyclonal antibody to p101-PI(3)K (07-281) and to $gp91^{phox}$ (07-024) and anti-Rac2 (07-604), biotin-labeled mouse mAb to phosphorylated tyrosine (4G10), as well as horseradish peroxidase–conjugated antibody to goat IgG (AP-180P) were from Upstate; fluorescein isothiocyanate–conjugated mouse mAb to gp91 (7D5) or goat antibody to mouse IgG (238) were from MBL; and mouse mAb to flotillin-1(18), $p67^{phox}$ (29) or PI(3)K-p85 (U15), and fluorescein isothiocyanate–conjugate mouse isotype-matched IgG antibody (MOPC-21) was from BD Pharmingen. Rabbit polyclonal antibody to PI(3)K-p85 (4292), to Lyn (2732), to Lyn phosphorylated at Tyr507 (2731), to Syk phosphorylated Tyr525-Tyr526 (2711), to Src phosphorylated Tyr416 (2101), to FAK phosphorylated Tyr576-Tyr577 (3281), to $p40^{phox}$ phosphorylated at Thr154 (4311) and to caspase-3 (9662), as well as mouse mAb to proliferating cell nuclear antigen (PC-19), were from Cell Signaling. Rabbit mAb to SOD1 (ep1727y), Mal (ep1231y) and catalase (ep1929), as well as rabbit polyclonal antibody to SOD2 (NB100-1992) and to Yes (NBP1-85369), were from Novus Biologicals. Rabbit polyclonal antibody to Bmx (ab73887), to Bmx phosphorylated at Tyr566 (ab59409), to Lyn phosphorylated at Tyr396 (EP503Y), to Vav phosphorylated at Tyr160 (ab4763) and to Prx1 (ab15571), and mouse mAb to Prx2 (12B1), as well as rabbit mAb to Btk (Y440), to CSK (CSK-04), to SHIP (EP378Y) and to Tec (Y398), were from Abcam. Rat mAb to Mal (TIRAP; sebi-1) was from ENZO Life Sciences. Goat polyclonal antibody to CBP (LS-C14699) was from LIFESPAN; anti-β-actin (Ab1) was from Calbiochem; and horseradish peroxidase–conjugated antibody to mouse IgG (NA931), to rabbit IgG (NA934) or to rat IgG (NA9350) was from GE Healthcare. Alexa Flour 546–anti–rabbit IgG (A11035), Alexa Flour 680–anti–rabbit IgG (A10043), Alexa Flour 594–anti–rat IgG (A21209) and Alexa Flour 488–anti–mouse IgG (A21202) were from Invitrogen. Mouse IgG (015-000-003) and rabbit IgG (011-00000-3) were from Jackson ImmunoResearch. Rat IgG2a (eBR2a) was from eBioscience. Horseradish peroxidase–conjugated streptavidin was from Cell Signaling.

The 482H mAb to Btk has been described[49]. Polyclonal antibody to human Btk was raised in rabbits with a Btk peptide of amino acids 169–187 (ENRNGSLKPGSSHRKTKKPC) conjugated to ovalubumin. The antibody collected was further affinity-purified with that same Btk peptide conjugated to thiol–Sepharose 4B (Pharmacia) and was used for immunoprecipitation in some experiments. The specificity of the antibody was confirmed by immunoblot analysis of lysates of Btk-deficient mononuclear cells. Antibody to phosphorylated Ser345 was generated in rabbits by injection of ovalbumin conjugated to a peptide of $p47^{phox}$ phosphorylated at Ser345 (QARPGPQSpPGSPLEEE, where 'Sp' indicates phosphorylated Ser345 (p-Ser345-pep)). The antibody raised was positively affinity-purified with activated thiol–Sepharose 4B adsorbed with p-Ser345-pep. The antibody was further purified by elimination of the fraction that bound to the same peptide of $p47^{phox}$ without phosphorylation at Ser345 (QARPGPQSPGSPLEEE (Ser345-pep)) by passage through thiol–Sepharose 4B conjugated to Ser345-pep; then, the antibody was used for immunoblot analysis. The specificity of the antibody was confirmed by direct enzyme-linked immunosorbent assay with plates coated with Ser345-pep or p-Ser345-pep and by immunoblot analysis experiments showing blockade of the p-$p47^{phox}$ signal by p-Ser345pep but not by Ser345-pep.

Subjects. Patients with XLA (n = 17) with stable health were studied (ages and Btk mutations, **Supplementary Fig. 3**). Healthy volunteers (n = 18) and patients with CVID (n = 5) were enrolled as healthy controls and disease control, respectively. Written informed consent was obtained from all subjects (or their parents). The study protocol was approved by the ethics committee of the Faculty of Medicine, Tokyo Medical and Dental University.

Isolation of neutrophils, monocytes and lymphocytes. Neutrophils were purified from heparinized peripheral blood by a standard technique. All samples were processed within 12 h of blood collection. Peripheral blood diluted in PBS was layered onto a MonoPoly mixture (Flow Laboratories) and centrifuged at 400*g* for 20 min. Layers with enrichment for neutrophils were collected and further purified to a purity of >97% by immunomagnetic negative selection (StemCell Technologies). Sterile and endotoxin-free conditions were used for all procedures. Monocytes were purified from the mononuclear cell–rich fraction with a human monocyte enrichment kit (StemCell Technologies), and lymphocytes were prepared as described[50].

Measurement of production of ROS. Purified neutrophils were loaded for 5 min at 37 °C with DHR123 (5 μg/ml). Cells were washed and then stimulated for 30 min at 37 °C with PMA (100 ng/ml), and the production of ROS was quantified via flow cytometry by measurement of intracellular rhodamine (FACSCalibur; Becton Dickinson). DHR123-loaded neutrophils were also stimulated for 60 min at 37 °C with a TLR ligand (lipopolysaccharide from *E. coli* or *P. aeruginosa*; 100 ng/ml), CpG-A (100 ng/ml) or TNF (1 μg/ml). After incubation, treated and untreated neutrophils were incubated for 5 min at 37 °C with or without fMLP (1 μM), followed by flow cytometry. Results are presented as MFI of treated cells – MFI of untreated cells.

Production of ROS was quantified by standard chemiluminescence. Neutrophils (1.0×10^6) were suspended in 0.5 ml PBS containing luminol (10 μM) preheated to 37 °C. After a baseline measurement was obtained, cells were stimulated with a TLR agonist and then with fMLP (1 μM) or with PMA (100 ng/ml); luminescence signals were monitored throughout the reaction.

Detection of apoptosis. Apoptotic cells were identified by staining with annexin V–fluorescein isothiocyanate and 7-AAD (7-amino-actinomycin D; BD Biosciences). Apoptosis was also identified by immunoblot analysis through the detection of cleaved caspase-3 or degraded proliferating cell nuclear antigen.

Flow cytometry. A FACSCalibur (Beckton Dickenson) was used for all flow cytometry analyzing surface expression of gp91, DHR123 staining, annexin V–7-AAD staining, and JC-1 mitochondrial membrane detection as described[50]. All analyses were undertaken after calibration of the fluorescence intensity with CaliBRITE Beads (BD Biosciences).

Subcellular fractionation of neutrophils. Isolated neutrophils were resuspended at a density of 5×10^7 cells per ml in ice-cold sonication buffer (HEPES (10 mM), pH 7.2, sucrose (0.15 M), EGTA (1 mM), EDTA (1 mM), NaF (25 mM), leupeptin (10 μg/ml), pepstatin (10 μg/ml), aprotinin (1 μg/ml) and PMSF (1 mM)). After sonication and pelleting on ice, 200 μl supernatant was layered on a discontinuous sucrose gradient consisting of 200 μl of 52% (wt/vol) sucrose, 200 μl of 40% (wt/vol) sucrose and 200 μl of 15% (wt/vol) sucrose. After centrifugation (100,000*g* for 60 min), 160 μl supernatant (cytosol source) and 120 μl interface of the 15%–40% sucrose layers (plasma-membrane source) were collected.

Immunoprecipitation and immunoblot analysis. Lysates were prepared from monocytes and lymphocytes as described[51]. For the preparation of lysates from neutrophils, cells were resuspended in lysis buffer (Tris-HCl (50 mM), pH 7.5, NaCl (150 mM), sucrose (0.25 M), EGTA (5 mM), EDTA (5 mM), leupeptin (15 μg/ml), pepstatin (10 μg/ml), aprotinin (10 μg/ml), PMSF (2.5 mM), 1.0% Nonidet-P40, 0.25% sodium deoxycholate, sodium pyrophosphate (10 mM), NaF (25 mM), Na_3VO_4 (5 mM), β-glycerophosphate (25 mM) and DNase I (1 μg/ml)), incubated for 30 min on ice and centrifuged at 15,000*g* for 30 min at 4 °C, then supernatants were collected. For extraction of the membrane-raft fraction, 1% n-dodecyl-β-D-maltoside was added to the lysis buffer. Immunoprecipitation and immunoblot analysis were done as described[52]. For immunoprecipitation of cytosolic proteins from neutrophils, cytosolic proteins

obtained as described above were diluted in four volumes of immunoprecipitation buffer (Tris-HCl (20 mM), pH 7.5, NaCl (150 mM), sucrose (0.25 M), EGTA (5 mM), EDTA (5 mM), leupeptin (15 μg/ml), pepstatin (10 μg/ml), aprotinin (10 μg/ml), PMSF (2.5 mM), 0.5% Triton-X, sodium pyrophosphate (10 mM), NaF (25 mM), Na_3VO_4 (5 mM), β-glycerophosphate (50 mM) and levamisole (1 mM)); supernatants were used for immunoprecipitation.

Measurement of phosphatidylinositol-(3,4,5)-trisphosphate. Phosphatidylinositol-(3,4,5)-trisphosphate in unstimulated neutrophils prepared from healthy controls and patients with XLA was measured with an enzyme-linked immunosorbent assay kit in accordance with the manufacturer's instructions (K-2500; Echelon).

Immunofluorescence staining. Cytospin preparations of neutrophils were air-dried and fixed for 10 min with paraformaldehyde in PBS, pH 7.4, then were made permeable for 20 min at −20 °C with acetone, washed, and incubated with the appropriate antibodies. After labeling and washing with 0.2% BSA in PBS, coverslips were mounted with Fluoromount G and the prepared specimens. Nuclei were counterstained with DAPI (4,6-diamidino-2-phenylindole). Slides were analyzed with a fluorescence microscope (FV10i; Olympus) equipped with Fluoview viewer and review station (Olympus). At least 100 cells were inspected for each slide.

Generation of Hph-1-Btk, Hph-1-Btk mutants, and transduction of recombinant protein into cells. Hph-1–tagged Btk constructs were generated by amplification of a full-length Btk cDNA fragment with the appropriate primers (**Supplementary Table 1a**). After the sequence of each PCR product was verified by DNA sequencing, the fragment was ligated into sites of a pET28b vector (Merck) cleaved by *Xma1* and *Sal1*; the vector has a six-histidine site for protein purification and two tandem Hph-1 sequences for protein transduction. Constructs with deletion of the Tec homology domain, SH3 domain or SH2 domain were generated by mutagenesis with the QuikChange SiteDirected Mutagenesis Kit (Stratagene) and the appropriate primers (**Supplementary Table 1b**). The Hph-1-Gal4 construct has been described[52]. Proteins were induced in BL21 Star competent cells (Novagen) as described[52]. Proteins were treated with Detoxi-Gel Endotoxin Removing Gel (Takara Bio) for elimination of endotoxins and were frozen at −80 °C until further use. Neutrophils (1×10^6 per ml) were incubated for 1 h with 1 μM Hph-1–tagged proteins (80 μg recombinant Hph-1–tagged full-length-Btk was used for 1×10^6 neutrophils for transduction at a concentration of 1 μM) and washed, then ROS production was assayed.

Btk-precipitation assay. Lysates of neutrophils from healthy controls were prepared on ice for 30 min with immunoprecipitation lysis buffer. Supernatants were then treated with protein G beads (GE Health Care) for removal of immunoglobulin G from the neutrophil lysate. For the Btk-precipitation assay, purified Btk recombinant proteins or control recombinant protein were eluted and proteins were measured by BCA protein assay (Pierce). Bacterial supernatants were bound to nickel–nitrilotriacetic acid Sepharose beads (Qiagen) and bound recombinant proteins were eluted, then equimolar amounts of recombinant proteins were rebound to the nickel beads; afterward, samples were washed and then incubated overnight at 4 °C with the cell lysates. Beads were washed four times with lysis buffer and assessed by immunoblot analysis with anti-Mal. Before incubation with cell lysates, the amount of the recombinant protein rebound to nickel beads was assessed by immunoblot analysis with anti-histidine, and the 'dose' was readjusted for further precipitation assays.

Statistical analysis. Student's *t*-test was used for statistical analysis. The software GraphPad Prism 4 was used for these analyses.

49. Futatani, T. *et al.* Deficient expression of Bruton's tyrosine kinase in monocytes from X-linked agammaglobulinemia as evaluated by a flow cytometric analysis and Its clinical application to carrier detection. *Blood* **91**, 595–602 (1998).
50. Takahashi, N. *et al.* Impaired CD4 and CD8 effector function and decreased memory T cell populations in ICOS-deficient patients. *J. Immunol.* **182**, 5515–5527 (2009).
51. Morio, T. *et al.* Ku in the cytoplasm associates with CD40 in human B cells and translocates into the nucleus following incubation with IL-4 and anti-CD40 mAb. *Immunity* **11**, 339–348 (1999).
52. Choi, J.M. *et al.* Intranasal delivery of the cytoplasmic domain of CTLA-4 using a novel protein transduction domain prevents allergic inflammation. *Nat. Med.* **12**, 574–579 (2006).

doi:10.1038/ni.2234

ELSEVIER

Experimental Hematology

Experimental Hematology 2012;40:477–486

The carboxyl-terminal region of erythroid-specific 5-aminolevulinate synthase acts as an intrinsic modifier for its catalytic activity and protein stability

Senkottuvelan Kadirvel[a], Kazumichi Furuyama[a], Hideo Harigae[b], Kiriko Kaneko[c], Yoshiko Tamai[d], Yoji Ishida[e], and Shigeki Shibahara[a]

[a]*Department of Molecular Biology and Applied Physiology;* [b]*Department of Hematology and Rheumatology;* [c]*Endocrinology and Applied Medical Science, Tohoku University School of Medicine, Sendai, Japan;* [d]*Division of Transfusion Medicine, Hirosaki University Hospital, Hirosaki, Japan;* [e]*Hematology and Oncology, Internal Medicine, Iwate Medical University School of Medicine, Morioka, Japan*

(Received 29 September 2010; revised 10 January 2012; accepted 18 January 2012)

Erythroid-specific 5-aminolevulinate synthase (ALAS2) is essential for hemoglobin production, and a loss-of-function mutation of ALAS2 gene causes X-linked sideroblastic anemia. Human ALAS2 protein consists of 587 amino acids and its carboxyl(C)-terminal region of 33 amino acids is conserved in higher eukaryotes, but is not present in prokaryotic ALAS. We explored the role of this C-terminal region in the pathogenesis of X-linked sideroblastic anemia. In vitro enzymatic activity was measured using bacterially expressed recombinant proteins. In vivo catalytic activity was evaluated by comparing the accumulation of porphyrins in eukaryotic cells stably expressing each mutant ALAS2 tagged with FLAG, and the half-life of each FLAG-tagged ALAS2 protein was determined by Western blot analysis. Two novel mutations (Val562Ala and Met567Ile) were identified in patients with X-linked sideroblastic anemia. Val562Ala showed the higher catalytic activity in vitro, but a shorter half-life in vivo compared to those of wild-type ALAS2 (WT). In contrast, the in vitro activity of Met567Ile mutant was about 25% of WT, while its half-life was longer than that of WT. However, in vivo catalytic activity of each mutant was lower than that of WT. In addition, the deletion of 33 amino acids at C-terminal end resulted in higher catalytic activity both in vitro and in vivo with the longer half-life compared to WT. In conclusion, the C-terminal region of ALAS2 protein may function as an intrinsic modifier that suppresses catalytic activity and increases the degradation of its protein, each function of which is enhanced by the Met567Ile mutation and the Val562Ala mutation, respectively. © **2012 ISEH - Society for Hematology and Stem Cells. Published by Elsevier Inc.**

5-Aminolevulinate synthase (ALAS) is the first and rate-limiting enzyme in the heme biosynthetic pathway [1]. There are two isozymes of ALAS in higher eukaryotes, ALAS1 and ALAS2. ALAS1 (alternatively, ALAS-N) is expressed ubiquitously in all types of nucleated cells, and expression of ALAS2 (or ALAS-E) is restricted in erythroid cells and essential for hemoglobin production during erythroid differentiation [1]. Both ALAS1 and ALAS2, which are encoded by the distinct nuclear genes, function in mitochondria [2,3], and the amino-terminal region of each isozyme acts as a targeting signal for mitochondrial translocation [4–6]. The remaining regions of ALAS protein consist of a core catalytic region and a carboxyl terminal (C-terminal) region, and the catalytic region is conserved among several species [7]. In addition, the C-terminal region of 33 amino acids (positions 555–587), which is encoded by the 11th exon of the human ALAS2 gene, is well conserved in higher eukaryotes, but the equivalent region is not present in bacterial ALAS [7]. It is conceivable that the C-terminal region of mammalian ALAS2 protein might have an important regulatory role in heme biosynthesis.

The human ALAS2 gene that is mapped on X chromosome consists of 11 exons [8], and a genetic mutation of the ALAS2 gene causes X-linked sideroblastic anemia (XLSA) [9,10] or X-linked dominant protoporphyria [11]. To the best of our knowledge, >50 different mutations of

Offprint requests to: Kazumichi Furuyama, M.D., Ph.D., Department of Molecular Biology and Applied Physiology, Tohoku University School of Medicine, 2-1 Seiryo-machi, Aoba-ku, Sendai, Miyagi 980-8575, Japan; E-mail: furuyama@med.tohoku.ac.jp

Supplementary data related to this article can be found online at doi: 10.1016/j.exphem.2012.01.013.

doi: 10.1016/j.exphem.2012.01.013

the ALAS2 gene have been identified in about 100 pedigrees with XLSA [12–14]. Reported mutations in patients with XLSA are distributed from the 5th exon to the 11th exon of the human ALAS2 gene, but only four mutations were detected in 11th exon [14–17]. In the case of X-linked dominant protoporphyria, two different frame-shift mutations have been identified in the 11th exon of the ALAS2 gene in two independent probands [11]. These frame-shift mutations cause deletions of 19 and 21 amino acids at the C-terminal end of ALAS2, both of which are accompanied by replacement of the C-terminal end with one unrelated amino acid and an unrelated peptide of 23 amino acids, respectively. Using recombinant proteins expressed in *Escherichia coli*, those authors provided evidence that deletion of 19 or 21 amino acids at C-terminal end increased the catalytic activity of ALAS2, suggesting that the C-terminal region can inhibit the enzymatic activity of ALAS2 [11]. Recently, it was also reported that the substitution (Tyr586Phe) at the penultimate amino acid of the C-terminal of ALAS2 increased its catalytic activity in vitro, which might be related to the severe phenotype of congenital erythropoietic porphyria [18]. Interestingly, such gain-of-function mutations of the ALAS2 gene were solely identified within the C-terminal region of ALAS2 protein. However, it is still unclear how the C-terminal region of ALAS2 is involved in the regulation of ALAS2 function in vivo.

Here, we report novel missense mutations in the 11th exon of the ALAS2 gene in independent probands with XLSA. Based on in vitro and in vivo functional studies of these mutants, as well as a C-terminal deletion mutant, we provide evidence that the C-terminal region of human ALAS2 protein reduces its catalytic activity and protein stability in mitochondria.

Case reports

Case 1

Japanese male proband presented with microcytic hypochromic anemia (hemoglobin: 8.1 g/dL; mean corpuscular volume: 57.7 fL) at age 14 years. Serum ferritin, serum iron, and total iron binding capacity were 222.7 ng/mL, 242 μg/dL, and 279 μg/dL, respectively. Proband's mother and maternal uncles had mild anemia, but they did not receive any medication for anemia.

Bone marrow examination of the patient showed erythroid hyperplasia (myeroid to erythroid ratio [M:E] = 0.45), with ringed sideroblasts comprising >10% of nucleated cells. Pyridoxine treatment (80 mg/d) was started, and the hemoglobin concentration gradually increased from 7.3 g/dL to 12.0 g/dL after 14 months.

Case 2

Japanese male proband was admitted to the hospital at age 36 years because of microcytic hypochromic anemia (hemoglobin: 6.5 g/dL; mean corpuscular volume: 64.4 fL) with systemic iron overload (ferritin: 2581.4 ng/mL). Anemia was pointed out before he was school age, but he did not receive any medication for anemia. Prussian blue staining of bone marrow cells revealed the presence of ring sideroblasts in the proband, and the diagnosis of sideroblastic anemia was established. Pyridoxine treatment (60 mg/d) was started when hemoglobin was 5.4 g/dL, then anemia was improved after 1 month to 9.9 g/dL hemoglobin. Although pyridoxine treatment was continued for an additional 4 months, the hemoglobin level did not exceed 10 g/dL.

Materials and methods

Reagents

Chemical reagents were purchased from Sigma-Aldrich (St Louis, MO, USA), Nacalai Tesque (Kyoto, Japan), or Wako Pure Chemicals (Osaka, Japan). Restriction enzymes and modifying enzymes used for construction of each plasmid were purchased from New England Biolabs (Ipswich, MA, USA), unless otherwise noted. ExTaq DNA polymerase and PrimeStar Max DNA polymerase were purchased from Takara Bio Inc. (Shiga, Japan) and were used for polymerase chain reaction (PCR) and site-directed mutagenesis, respectively. Protein concentration was measured with Bio-Rad Protein assay reagent (Bio-Rad Laboratories Inc., Hercules, CA, USA) or Pierce 660 nm Protein Assay Reagent (Thermo Scientific, Rockford, IL, USA) using bovine serum albumin as a standard. Sodium dodecyl sulfate polyacrylamide electrophoresis (SDS-PAGE) and Western blot analysis were performed as described previously [19]. Prestained XL-ladder broad range (APRO Science, Tokushima, Japan) was loaded as a size marker for SDS-PAGE and Western blot analysis.

Identification of ALAS2 mutations

Genetic analyses performed in this project had been approved by the ethical committee of Tohoku University School of Medicine. Blood samples were drawn from the probands and the family members after informed consent. Genomic DNA was then extracted from them using QIAamp DNA Blood Midi Kit (Qiagen GmbH, Hilden, Germany). All exons including exon-intron boundaries, the proximal promoter region, and the erythroid enhancer in intron 8 of ALAS2 gene were amplified using ExTaq DNA polymerase. Sequences of primers and the condition for PCR were reported previously [20], except for an antisense primer for exon 5 and a primer pair for the erythroid-specific enhancer region in intron 8. The sequence of antisense primer for exon 5 used is (5′-TCATCTCCTCTGGCCACTGC-3′). For the amplification of the erythroid-specific enhancer in intron 8, the following primers were used: sense, 5′-GGTACCACTCGCATCCCACTGCA GAG-3′and antisense, 5′-GGTACCACACAGCCAAAGGCCTT GCC-3′. Each amplified DNA fragment was electrophoresed on 1% agarose gel in TAE buffer and stained with ethidium bromide. DNA fragment was excised from the gel for purification using QIAquick Gel Extraction Kit (Qiagen GmbH). Purified DNA fragment was directly sequenced using BigDye terminator v1.1 cycle sequencing kit and ABI 3100 Genetic Analyzer (Applied Biosystems, Foster City, CA, USA). The same primers were used for PCR and direct sequencing analysis. Sequencing results were

analyzed using Lasergene software (DNASTAR Inc., Madison, WI, USA), and the mutation of ALAS2 gene was confirmed by repeated amplification and direct sequencing.

Expression and purification of recombinant ALAS2 proteins

Complementary DNA for human mature ALAS2 that lacks the amino-terminal region was amplified with PrimeStar Max DNA polymerase (Takara Bio Inc.) using the following primers (sense, 5′-GGTGGTCATATGATCCACCTTAAGGCAACAAAGG-3′; antisense, 5′-GGCATAGGTGGTGACATACTG-3′), each of which was phosphorylated at its 5′ end beforehand. Amplified complementary DNA (cDNA) was digested with NdeI restriction enzyme, and was cloned between NdeI site and blunt ended SapI site of pTXB1 expression vector (New England Biolabs). Resulting plasmid, named as pTXB1-AEm, expresses human mature ALAS2 in *E. coli* as a fusion protein with Intein tag and Chitin binding domain at its C-terminal end. Using pTXB1-AEm as a template, each mutation or deletion was introduced using PrimeStar Max site-directed mutagenesis kit (Takara Inc.). The sequences of primers used for mutagenesis are available upon request. After the amplification of cDNA or mutagenesis, the sequence of mature ALAS2 cDNA and the junction sequence for fusion protein was confirmed by DNA sequencing before use. These expression vectors were used for transformation of the *E. coli* strain, BL21(DE3). Expression and purification of recombinant proteins were performed according to manufacturer's instruction for Impact System (New England Biolabs), with minor modifications. Briefly, expression of recombinant proteins was induced in *E. coli* with 0.1 mM isopropyl β-D-1-thiogalactopyranoside at 25°C for overnight. The isopropyl β-D-1-thiogalactopyranoside–treated cells were collected by centrifugation and resuspended with lysis buffer (20 mM Tris-HCl [pH 8.5], 300 mM NaCl, 1 mM EDTA, 0.1% Triton X-100, 1 mM phenylmethanesulfonyl fluoride, 1 μg/mL antipain, 1 μg/mL pepstatin, and 1 μg/mL leupeptin). After sonication and centrifugation, cleared cell lysates were incubated with Chitin beads for 1 hour at 4°C, and then washed with wash buffer (20 mM Tris-HCl [pH 8.5], 500 mM NaCl, 1 mM EDTA, and 0.1% Triton X-100). To obtain a tag-free recombinant mature ALAS2 protein, on-column cleavage was induced with 50 mM dithiothreitol in wash buffer at room temperature for 16 hours. After the elution from the column, each recombinant protein was dialyzed against wash buffer before use. Purity of each recombinant protein was examined using SDS-PAGE, followed by staining with Quick-CBB PLUS (Wako Pure Chemical). Enzymatic activity of each recombinant protein was measured according to the protocol described previously [21]. Student's *t* test was performed for statistical analysis.

Expression of wild-type or mutant ALAS2 protein in eukaryotic cells

The plasmid "pGEM-AET," which carries cDNA for full-length ALAS2 tagged with FLAG at its C-terminal, was described previously [22]. Site-directed mutagenesis was performed by PrimeStar Max mutagenesis kit (Takara Inc.) using pGEM-AET as a template to obtain cDNA encoding each FLAG-tagged mutant. In addition, cDNA encoding FLAG-tagged luciferase protein was constructed by replacing ALAS2 cDNA in pGEM-AET with amplified luciferase cDNA derived from pGL3 basic (Promega Corporation, Madison, WI, USA).

For establishing the stable transformants in which expression of FLAG-tagged ALAS2 protein or FLAG-tagged luciferase protein is inducible with tetracycline, cDNA for each protein was cloned into pcDNA5/FRT/TO vector (Invitrogen Corporation, Carlsbad, CA, USA). The resulting cDNA construct was then co-introduced with pOG44 vector into Flp-In T-REx 293 cells (Invitrogen), derived from human embryonic kidney cells (HEK293). After transfection, cells were incubated with 100 μg/mL Hygromycin B (Wako Pure Chemicals) and 15 μg/mL Blasticidin (Invitrogen). At least three independent clones, which were resistant to Hygromycin B and sensitive to Zeocin (Invitrogen), were selected and expanded for subsequent experiments. This phenotype of a given clone confirmed the integration of each cDNA expression cassette into the expected site in the genome of Flp-In T-REx 293 cell line.

For the determination of protein stability, expression of wild-type ALAS2 or mutant ALAS2 was induced by the addition of tetracycline into the culture medium (final concentration of 1 μg/mL) for 48 or 72 hours, and then the culture medium was replaced with fresh complete medium containing tetracycline with or without 10 μM cycloheximide. At 0, 3, 6, 9, and 12 hours after incubation, cells were harvested and lysed in RIPA buffer (10 mM Tris-HCl [pH 7.2], 150 mM NaCl, 1% TritonX-100, 1 mM sodium fluoride, 0.4 mM Na_3VO_4, 10 mM N-ethylmaleimide, 1 mM phenylmethanesulfonyl fluoride, 2 μg/mL leupeptin, and 2 μg/mL aprotinin). Cell lysates were centrifuged at 13,200*g* for 10 minutes at 4°C, and the supernatants were used for SDS-PAGE. Expression of FLAG-tagged ALAS2 protein was detected by Western blot analysis with anti-FLAG M2 monoclonal antibody (Sigma-Aldrich) as a first antibody. For normalization of loaded samples, glyceraldehyde-3-phosphate dehydrogenase (GAPDH) was detected with anti-GAPDH monoclonal antibody (MAB374; Millipore Corporation, Billerica, MA, USA) as a first antibody. For a second antibody, horseradish peroxidase–conjugated anti-mouse IgG (NA931Vl GE Healthcare, UK Limited, Buckinghamshire, UK) was used. Intensity of each band was measured using ImageJ software (available at http://rsb.info.nih.gov/ij/). The intensity of each band for FLAG-tagged ALAS2 was normalized with that of GAPDH, and the normalized intensity of FLAG-tagged ALAS2 at each time point was compared with that of the sample harvested at 0 hour. We repeated this series of experiments three times for each clone, and an average of these results was used for determination of the half-life of each protein.

The catalytic activity of each mutant protein was also evaluated by comparing the accumulation of porphyrins in Flp-In T-Rex 293 cells that expressed wild-type or mutant ALAS2 cDNA in an inducible manner. For this assay, cells of low-passage numbers (between passage 5 and passage 15) were used for obtaining reproducible results. To induce expression of wild-type ALAS2 or mutant ALAS2 protein in isolated cell lines, cells were treated for 60 hours with tetracycline at a suitable concentration (12.5–50 ng/mL), depending on cell lines. Then, cells were washed with phosphate-buffered saline twice and collected in the sample tube. Flp-In T-REx 293 cells, which express FLAG-tagged luciferase protein in an inducible manner, were also treated with tetracycline as a negative control. Cells were separately collected for Western blot analysis and RNA preparation. Real-time PCR analysis was performed as described previously [23]. Remaining cells were collected by centrifugation and then packed cells were exposed to ultraviolet light for detection of porphyrins.

Table 1. Summarized features of recombinant ALAS2 proteins

Recombinant protein	In vitro enzymatic activity (nmol ALA/mg protein/h)			Half-life in HEK293 cells (h)	Porphyrin accumulation in HEK293 cells
	Without PLP (% of wild-type)	With 200 μM PLP (% of wild-type)	Ratio with/without PLP		
Wild-type	14,824 ± 754 (100%)	27,627 ± 713 (100%)	1.86	7.8	+++
Val562Ala	22,324 ± 1,555 (150.6%)	32,300 ± 709 (116.9%)	1.44	5.3	++
Met567Ile	5,653 ± 897 (38.1%)	6,975 ± 299 (25.2%)	1.23	>12	±
Ser568Gly*	(19.5%)*	(31.6%)*	2.51*	>12	±
delC33	15,769 ± 382 (106.4%)	53,066 ± 1,843 (192.1%)	3.37	>12	++++

*Data with GST-fused Ser568Gly protein taken from reference [15].

Results

Identification of novel mutations of ALAS2 gene

Analyzing the genomic DNA extracted from the proband of case 1, we identified the c.T1685C mutation in the 11th exon of ALAS2 gene (Supplementary Figure E1A, upper panel; online only, available at www.exphem.org). This transition results in an amino acid substitution at the 562nd residue of ALAS2 protein from valine to alanine (Val562Ala). The same mutation was identified in one allele of the proband's mother (Supplementary Figure E1A, middle panel; online only, available at www.exphem.org), and the proband's father does not carry this mutation (Supplementary Figure E1A, lower panel; online only, available at www.exphem.org), indicating the X-linked inheritance of this mutation. For the proband of case 2, the c.G1701C transversion was identified in exon 11 of ALAS2 gene (Supplementary Figure E1B; online only, available at www.exphem.org), the mutation of which results in an amino acid substitution at the 567th residue from methionine to isoleucine (Met567Ile).

To exclude the possibility that these mutations represent single nucleotide polymorphisms, we examined the 11th exon of ALAS2 gene in 96 Japanese healthy volunteers (57 male and 39 female subjects, with the total allele number of 135) using PCR followed by direct sequencing. As a result, no base change was found in the 11th exon of ALAS2 gene in these subjects, suggesting that the mutation found in each proband might not represent single nucleotide polymorphism. It is therefore conceivable that either the c.T1685C or c.G1701C mutation might be responsible for XLSA.

Enzymatic activities of mutant ALAS2 proteins in vitro

Wild-type ALAS2 or each mutant ALAS2 protein was expressed in *E. coli* and purified as a tag-free protein. The combination of pTXB1 expression vector and IMPACT system allowed us to obtain a tag-free/C-terminal intact recombinant protein. Indeed, modified Coomassie Brilliant Blue staining of the gel after SDS-PAGE revealed that the purity of each prepared protein was >95% (data not shown). These recombinant proteins were suitable for determination of the catalytic activity of each mutant protein that carries the amino acid substitution near the C-terminal end.

We measured the catalytic activity of each recombinant ALAS2 protein with or without pyridoxal 5-phosphate (PLP). Data are summarized in Table 1. Unexpectedly, the catalytic activity of Val562Ala protein was significantly higher than that of wild-type protein ($p = 0.0046$), when the activity was measured without PLP in the assay mixture. In addition, in the presence of 200 μM PLP, Val562Ala mutant showed significantly higher activity than that of wild-type ALAS2 ($p = 0.0087$). In contrast, the catalytic activity of Met567Ile protein was lower than that of wild-type protein, irrespective of without PLP ($p = 0.0011$) or with PLP ($p = 0.0003$). It is also noteworthy that the PLP-associated increases in enzymatic activities were 86%, 44%, and 23% for wild-type, Val562Ala, and Met567Ile proteins, respectively, suggesting that Val562Ala and Met567Ile mutations decreased the responsiveness to PLP (Table 1). The lowest PLP responsiveness of Met567Ile mutant protein might account for the clinical course of the proband in case 2; that is, the anemia of this proband was improved only marginally, despite pyridoxine treatment.

Because we previously reported on the Ser568Gly mutation [15], which is also located in the C-terminal region of human ALAS2 protein, the reported data for the Ser568Gly mutation were included as a reference in Table 1. In vitro enzymatic activity of glutathione *S*-transferase (GST)–fused Ser568Gly was significantly lower than that of the GST–fused wild-type ALAS2 with or without PLP [15]. Therefore, the functional consequence of amino acid substitution at Ser568 was similar to that of Met567Ile (Table 1). In addition, the degree of PLP-mediated increase in Ser568Gly activity, indicated as "ratio with/without PLP" in Table 1, was larger than that with wild-type protein, although the possibility remains that the GST tag might have influenced the PLP responsiveness of a recombinant ALAS2 protein. We, therefore, included Ser568Gly mutant in subsequent analyses.

The higher catalytic activity of Val562Ala protein prompted us to examine the function of the C-terminal region of ALAS2 protein. We measured the enzymatic

activity of the deletion mutant that lacks the 33 amino acids at the C-terminal end (positions 555–587) of human ALAS2 (delC33 mutant), the region of which was conserved among mammalian ALAS2 proteins, including Val562. As shown in Table 1, the enzymatic activity of the delC33 mutant was higher by two times in the presence of PLP than that of wild-type ALAS2 ($p = 0.002$), whereas they showed similar enzymatic activity in the absence of PLP. These results suggest that the 33 amino acids at the C-terminal end of human ALAS2 protein might repress the enzymatic activity, probably by interfering with the access of PLP cofactor to the catalytic site.

Stability of mutant ALAS2 proteins in vivo

We were interested in studying how the Val562Ala mutation is associated with XLSA, despite higher enzymatic activity. We examined the stability of the Val562Ala mutant protein and other C-terminal mutant proteins in vivo. When human ALAS2 protein is expressed as a FLAG-tagged protein in eukaryotic cells, the precursor and mature proteins should be detected as 65.7-kDa and 60.5-kDa proteins, respectively. As shown in Figure 1B (upper panel) and Figure 2 (middle panel), FLAG-tagged wild-type ALAS2 and mutant ALAS2 proteins, except for delC33 mutant, were detected as bands at about 60 kDa, an expected size of the mature protein. These results suggest that the leader peptide at the N-terminal end was cleaved after translocation of the precursor protein into mitochondria [4]. In fact, the precursor protein was detected at an expected size, when HeLa cells were transfected with FLAG-ALAS2 expression vector, and then incubated with hemin (Supplementary Figure E2; online only, available at www.exphem.org), which is known to inhibit mitochondrial translocation of ALAS precursor protein into mitochondria [4]. Based on our experiments (Fig. 1A–C), the half-lives of wild-type and Val562Ala mature proteins in mitochondria were calculated as 7.8 hours and 5.3 hours, respectively. The half-life of the Val562Ala mutant protein (Fig. 1C) is shorter than that of wild-type ALAS2 protein (Fig. 1B). In contrast, the half-life of Met567Ile (Fig. 1D) or Ser568Gly (Fig. 1E) mutant was not measurable by our experiments because the 50% reduction of the protein level was not observed within 12 hours for these mutants. Thus, the half-lives of Met567Ile and Ser568Gly mutants were longer than 12 hours. Importantly, the amino acid substitutions in the C-terminal region influenced the stability of the mature ALAS2 protein in mitochondria in different manners. Namely, Val562Ala mutation results in destabilization of the mature protein, and either Met567Ile or Ser568Gly mutation stabilizes the mature protein in mitochondria.

In addition, we measured the half-life of delC33 mutant in HEK293-derived cells (Fig. 1F), showing that the 50% reduction was not observed within 12 hours, which was similar to Met567Ile and Ser568Gly mutants. These results suggested that the 33 amino acids at C-terminal region of ALAS2 protein suppressed the catalytic activity in vitro, as well as protein stability in mitochondria. Our data also indicate that Val562Ala mutation might enhance the destabilization function of the C-terminal region, whereas Met567Ile and Ser568Gly mutations might enhance the suppressive function for enzymatic activity.

Enzymatic activity of each ALAS2 mutant protein in vivo

Val562Ala mutant showed higher enzymatic activity in vitro (Table 1), but it was less stable in mitochondria (Fig. 1A) compared with wild-type ALAS2. On the other hand, Met567Ile and Ser568Gly mutants showed lower enzymatic activities in vitro (Table 1), with prolonged half-lives in mitochondria (Fig. 1A). We, therefore, determined the catalytic activity of each mutant protein in vivo. For this purpose, we compared the accumulation of porphyrins in HEK293-derived cells that expressed wild-type protein or a mutant protein, as we described previously [20]; that is, the accumulation of porphyrins was evaluated by comparing the intensity of the fluorescence under ultraviolet light (Fig. 2, upper panel). The accumulation of porphyrins was detected in cells expressing wild-type ALAS2, but not in cells expressing tagged luciferase. These results indicate that FLAG-tagged ALAS2 is catalytically active in mitochondria. In contrast, the accumulation of porphyrins was decreased in cells expressing Val562Ala, Met567Ile, or Ser568Gly protein, compared to cells expressing wild-type ALAS2. Among these three missense mutations, Val562Ala mutant showed higher catalytic activity than did Met567Ile or Ser568Gly mutant (Fig. 2, upper panel). In addition, the highest porphyrin accumulation was observed in cells expressing delC33. Of note, the expression level of Val562Ala mutant protein was much lower than that of any other mutant or wild-type ALAS2, as judged by Western blot analysis (Fig. 2, middle panel), although there was no significant difference in relative expression level of each mutant ALAS2 messenger RNA (Fig. 2, lower panel). These results suggest that Val562Ala mutant protein is catalytically hyperactive but unstable in mitochondria, which is consistent in part with the higher enzymatic activity detected in vitro (Table 1) and with the short-half life in vivo (Fig. 1A).

In conclusion, Val562Ala, Met567Ile, or Ser568Gly ALAS2 has lower enzymatic activity in mitochondria compared with the activity of wild-type ALAS2. Therefore, these three mutations are categorized as a loss-of-function mutation and are responsible for sideroblastic anemia.

Discussion

It is well known that a loss-of-function mutation of the ALAS2 gene causes XLSA. In addition to the ALAS2 gene, other genes (e.g., SLC25A38 [24], GLRX5 [25], ABCB7 [26], PUS1 [27], SLC19A2 [28], and mitochondrial DNA [29]) were reported to be responsible for

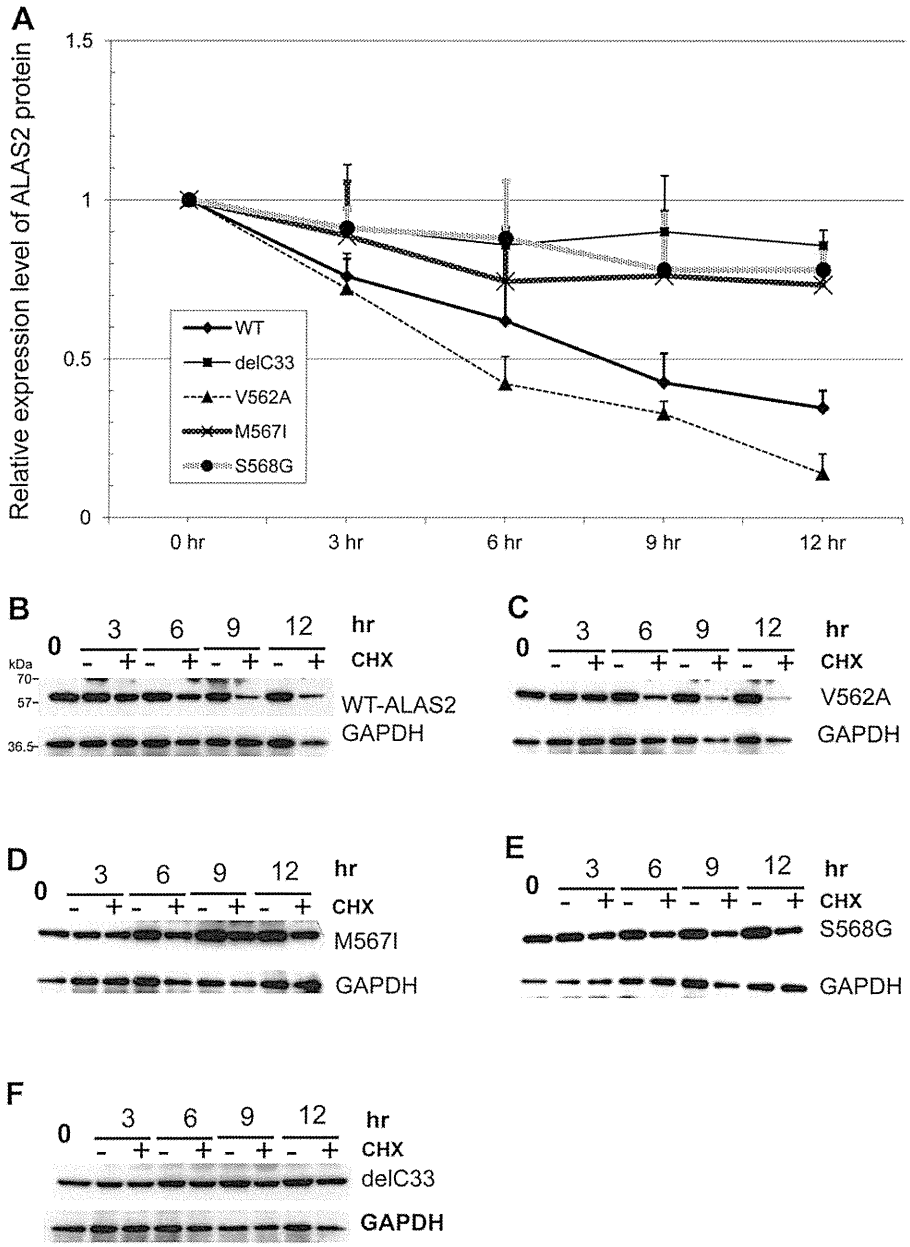

Figure 1. Effect of cycloheximide on FLAG-tagged ALAS2 protein level in eukaryotic cells. Expression of each FLAG-tagged protein was induced with tetracycline (1 μg/mL) in HEK293-derived cells for 48 hours, and then cells were treated with 10 μg/mL cycloheximide (CHX) for the indicated hours. Cells were collected and lysed in RIPA buffer, and FLAG-tagged proteins were detected by Western blot analysis (**B**–**F**). The intensity of the FLAG-tagged protein was normalized with the intensity of GAPDH for each time point. In (**A**), the relative intensity representing FLAG-tagged protein at 0 hours was considered to be 100%. The half-life of each protein was calculated on the basis of 50% reduction of each protein expression from the relative expression curves obtained from the samples with CHX. Average value of three independent experiments was used for preparing (**A**). Representative data of each ALAS2 protein are shown (**B**–**F**): (**B**) wild-type (WT) ALAS2; (**C**) Val562Ala; (**D**) Met567Ile; (**E**) Ser568Gly; and (**F**) delC33.

hereditary or congenital sideroblastic anemia. Among these candidate genes, mutations in ALAS2 gene are most frequently identified in patients with sideroblastic anemia [30], but characterization of each mutant ALAS2 protein was not fully performed. To the best of our knowledge, 24 of 56 mutations of the ALAS2 gene were characterized in vitro using recombinant proteins with or without a peptide-tag [9,10,14,15,20,21,31–36]. In the 11th exon of the ALAS2 gene, Ser568Gly [15], Arg559His [17], Arg560His [16], and Arg572His [14] mutations have been reported; however, only Ser568Gly and Arg572His mutants were characterized using recombinant proteins. Concerning the Ser568Gly mutation [15], we confirmed that Ser568Gly mutation resulted in decreased enzymatic activity in vitro (about 30% of wild-type with PLP in the assay mixture), as shown in Table 1. In contrast, Ducamp et al. [14] were

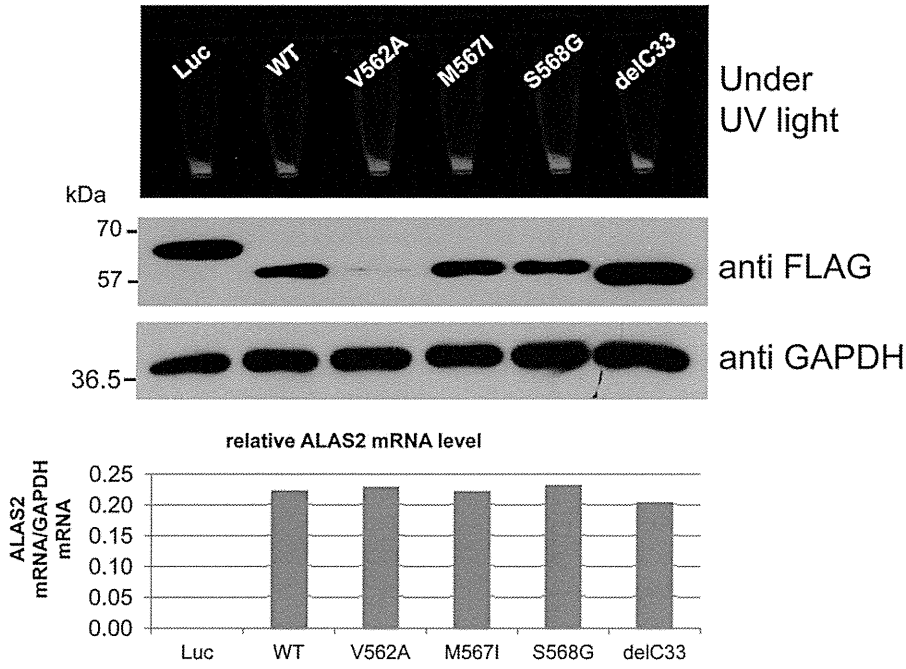

Figure 2. Evaluation of porphyrin production in cells expressing each ALAS2 mutant protein. Each FLAG-tagged ALAS2 protein or FLAG-tagged luciferase protein as a control was expressed in Flp-In T-REx 293 cells. Accumulation of porphyrins in each cell line was visualized by ultraviolet light exposure (upper panel). Expression levels of each FLAG-tagged protein and GAPDH (loading control) were detected by Western blot analysis (middle panels). Expression level of ALAS2 messenger RNA (mRNA) was measured by real-time PCR, and it was normalized with the expression level of GAPDH mRNA. Note that the data confirm the similar mRNA level of each ALAS2 protein (lower panel).

unable to determine the defect of the Arg572His mutant using an in vitro system because the mutant protein showed the enzymatic activity similar to that of wild-type ALAS2.

Measurement of enzymatic activity of every recombinant protein in vitro is one of the most useful techniques to characterize a mutant ALAS2 protein. Met567Ile mutant showed lower enzymatic activity than did wild-type protein (see Fig. 2), suggesting that this mutation causes sideroblastic anemia. In contrast, we were unable to uncover the pathogenesis of Val562Ala mutant protein using this in vitro assay system, indicating a limitation of the in vitro assay system with a bacterially expressed recombinant protein. In fact, using the in vivo system (Fig. 2), we have successfully demonstrated that the Val562Ala mutant protein showed lower porphyrin accumulation due to enzyme instability compared to wild-type ALAS2. In addition, the half-life of mature Val562Ala protein (5.3 hours) was shorter than that of wild-type ALAS2 (7.8 hours) (Fig. 1), suggesting that Val562Ala mutation altered the protein stability in mitochondria. These in vivo methods seem to be useful to characterize a mutant protein that does not show decreased enzyme activity in the in vitro assay system.

It is of particular interest that the Val562Ala and Met567Ile mutants exerted opposite effects on the enzymatic activity in vitro (Table 1) and on the protein stability in mitochondria (Fig. 1). In this connection, the deletion of 33 amino acids at C-terminal end of ALAS2 protein, the region of which contains Val562 and Met567 residues, resulted in higher enzymatic activity in vitro and in vivo (Table 1) and stable protein with a longer half-life in mitochondria (Fig. 1). The C-terminal region has a suppressive function on enzymatic activity, as well as protein stability in mitochondria. Because this region is conserved in eukaryotic ALAS2 but is absent in prokaryotic ALAS, the suppressor domain might be involved in the functional regulation of ALAS2 in mitochondria. In fact, in the C-terminal region, two frame-shift mutations of the ALAS2 gene were reported to cause X-linked dominant protoporphyria [11], and six (including present two cases) missense mutations were identified in patients with XLSA. In addition, it was recently reported that the Tyr586Phe mutation of ALAS2 protein increased the enzymatic activity, which can contribute to the severe clinical phenotype of the patient with congenital erythropoietic porphyria [18]. These results suggest that the C-terminal region of ALAS2 functions as an intrinsic suppressor for protoporpyrin production in erythroid cells.

It is still unclear how this C-terminal region suppresses the enzymatic activity of ALAS2 protein in mitochondria. It has been reported that certain amino acids are essential for catalytic activity of mouse Alas2 [18,37–45]. However, only limited information is available concerning the role of the C-terminal region in the catalytic activity of ALAS2. To-Figueras et al. [18] performed the stoichiometric analysis of the mature ALAS2 protein to characterize Tyr586-Phe mutant, which was reported as a gain-of-function

mutation at the penultimate C-terminal amino acid of ALAS2 protein. Steady-state kinetic analyses revealed that Tyr586Phe mutant showed higher catalytic activity with greater catalytic efficiency for glycine and succinyl-CoA than those of wild-type ALAS2. In addition, these authors provided evidence that the Tyr586Phe mutant enzyme was able to form and release ALA more rapidly than wild-type enzyme. Similar mechanisms might underlie the increased activity of every C-terminal deletion mutant, including the mutant ALAS2 protein with the deletion of 19 or 21 amino acids [11] and the delC33 mutant. In addition, the delC33 mutant expressed enzymatic activity similar to wild-type ALAS2 without PLP in assay mixture, but its enzymatic activity was increased about twofold compared to the wild-type with PLP (Table 1). These results suggest that this region might be involved in efficient use of PLP or accessibility of PLP to the catalytic site.

Crystal structure analysis of homodimeric ALAS from Rhodobactor capsulatus ($ALAS_{RC}$) revealed that $ALAS_{RC}$ showed open or closed structure, which was related to the conformational change of the active site loop [17]. This active site loop consists of evolutionally conserved structure at the C-terminal region of $ALAS_{RC}$, and seems to cover the catalytic site, which is located at the homodimer interface of ALAS protein. It should be noted that $ALAS_{Rc}$ does not contain the C-terminal region equivalent to that of mammalian ALAS2 [17]. The open conformation was observed only in the substrate-free $ALAS_{RC}$ protein, and the closed conformation was observed in $ALAS_{RC}$ protein that bound glycine and succinyl-CoA. To clarify the functional consequence of the conformational change of this active site loop, Lendrihas et al. introduced a mutation into nonconserved amino acid at this active site loop in mouse Alas2 protein and obtained several hyperactive variants [46]. Pre–steady-state kinetic analysis revealed that release of ALA from the catalytic site of the enzyme, which is coincident with opening of the active site loop [45], was accelerated in these hyperactive variants. Because the release of ALA from catalytic site is the rate-limiting step of enzymatic reaction of ALAS [47], these results suggest that the dynamic conformational change of this active site loop might control the rate of the reaction. Importantly, the accelerated release of ALA from the enzyme was also proposed in Tyr586Phe mutant [18]. It is therefore possible that the C-terminal domain of human ALAS2 protein is involved in the regulation of the conformational change of the active site loop.

In the present study, we determined the stability of ALAS2 protein in vivo, although the protein was tagged with a small peptide and expressed in HEK293-derived cells. Based on our assay condition, the half-life of human ALAS2 mature protein is 7.8 hours; however, it is not clear whether this result is comparable with that of the native ALAS2 protein in erythroid mitochondria, which has never been reported. On the other hand, this assay revealed that the stability of the Val562Ala mutant protein was decreased in mitochondria (Fig. 1), although the in vitro assay using purified recombinant protein failed to detect the unstable property of this mutant. In addition, our in vivo assay system clearly showed that the C-terminal region of 33 amino acids of human ALAS2 protein suppressed the enzymatic activity and decreased the protein stability. It is also interesting that the Val562Ala mutation and the Met567Ile mutation have opposite effects on the two functions of the C-terminal region. These results suggest that independent mechanisms might be involved in the reduction of enzymatic activity and destabilization in mitochondria. Taken together, the C-terminal region of ALAS2 protein can decrease catalytic activity by altering the open or closed structure of the catalytic site, while the post-translational modification of the C-terminal region, which is induced by a certain intracellular condition (e.g., increased or decreased oxidative stress) or by the association with other molecules, can enhance the disappearance of ALAS2 protein from mitochondria. The crystal structure of ALAS from $ALAS_{RC}$ provided critical information about the mechanisms for catalytic reaction of ALAS [45,46]. However, determination of the crystal structure of mammalian ALAS2 should await additional investigation on the function of the C-terminal region of ALAS2 protein.

Funding disclosure

This work was supported in part by a Grant-in-Aid for Scientific Research (C) (to K. Furuyama) and Health and Labour Sciences Research Grants (to H. Harigae).

Acknowledgment

We are also grateful to Biomedical Research Core of Tohoku University Graduate School of Medicine for allowing us to use various facilities.

Conflict of interest disclosure

No financial interest/relationships with financial interest relating to the topic of this article have been declared.

References

1. Anderson KE, Sassa S, Bishop DF, Desnick RJ. Disorders of heme biosynthesis: X-linked sideroblastic anemia and the porphyrias. In: Scriver CR, Beaudet AL, Sly WS, Valle D, eds. The Metabolic & Molecular Bases of Inherited Disease. New York: McGraw-Hill Medical Publishing Division; 2001. p. 2991–3062.
2. Hayashi N, Yoda B, Kikuchi G. Difference in molecular sizes of delta-aminolevulinate synthetases in the soluble and mitochondrial fractions of rat liver. J Biochem. 1970;67:859–861.
3. Bishop DF, Henderson AS, Astrin KH. Human delta-aminolevulinate synthase: assignment of the housekeeping gene to 3p21 and the erythroid-specific gene to the X chromosome. Genomics. 1990;7: 207–214.

4. Lathrop JT, Timko MP. Regulation by heme of mitochondrial protein transport through a conserved amino acid motif. Science. 1993;259: 522–525.
5. Munakata H, Sun JY, Yoshida K, et al. Role of the heme regulatory motif in the heme-mediated inhibition of mitochondrial import of 5-aminolevulinate synthase. J Biochem. 2004;136:233–238.
6. Dailey TA, Woodruff JH, Dailey HA. Examination of mitochondrial protein targeting of haem synthetic enzymes: in vivo identification of three functional haem-responsive motifs in 5-aminolaevulinate synthase. Biochem J. 2005;386:381–386.
7. Munakata H, Yamagami T, Nagai T, Yamamoto M, Hayashi N. Purification and structure of rat erythroid-specific delta-aminolevulinate synthase. J Biochem. 1993;114:103–111.
8. Cox TC, Bawden MJ, Abraham NG, et al. Erythroid 5-aminolevulinate synthase is located on the X chromosome. Am J Hum Genet. 1990;46:107–111.
9. Cox TC, Bottomley SS, Wiley JS, Bawden MJ, Matthews CS, May BK. X-linked pyridoxine-responsive sideroblastic anemia due to a Thr388-to-Ser substitution in erythroid 5-aminolevulinate synthase. N Engl J Med. 1994;330:675–679.
10. Cotter PD, Baumann M, Bishop DF. Enzymatic defect in "X-linked" sideroblastic anemia: molecular evidence for erythroid delta-aminolevulinate synthase deficiency. Proc Natl Acad Sci U S A. 1992;89:4028–4032.
11. Whatley SD, Ducamp S, Gouya L, et al. C-terminal deletions in the ALAS2 gene lead to gain of function and cause X-linked dominant protoporphyria without anemia or iron overload. Am J Hum Genet. 2008;83:408–414.
12. Bottomley SS. Sideroblastic anemias. In: Greer JP, Foerster J, Rogers GM, et al., eds. Wintrobe's Clinical Hematology. 12th ed. Philadelphia/London: Wolters Kluwer Health/Lippincott Williams & Wilkins; 2009. p. 835–856.
13. Harigae H, Furuyama K. Hereditary sideroblastic anemia: pathophysiology and gene mutations. Int J Hematol. 2010;92:425–431.
14. Ducamp S, Kannengiesser C, Touati M, et al. Sideroblastic anemia: molecular analysis of the ALAS2 gene in a series of 29 probands and functional studies of 10 missense mutations. Hum Mutat. 2011; 32:590–597.
15. Harigae H, Furuyama K, Kimura A, et al. A novel mutation of the erythroid-specific delta-aminolaevulinate synthase gene in a patient with X-linked sideroblastic anaemia. Br J Haematol. 1999;106:175–177.
16. Cazzola M, May A, Bergamaschi G, Cerani P, Ferrillo S, Bishop DF. Absent phenotypic expression of X-linked sideroblastic anemia in one of 2 brothers with a novel ALAS2 mutation. Blood. 2002;100: 4236–4238.
17. Astner I, Schulze JO, van den Heuvel J, Jahn D, Schubert WD, Heinz DW. Crystal structure of 5-aminolevulinate synthase, the first enzyme of heme biosynthesis, and its link to XLSA in humans. EMBO J. 2005; 24:3166–3177.
18. To-Figueras J, Ducamp S, Clayton J, et al. ALAS2 acts as a modifier gene in patients with congenital erythropoietic porphyria. Blood. 2011;118:1443–1451.
19. Sambrook J, Russell DW. Molecular Cloning: A Laboratory Manual. 3rd ed. Cold Spring Harbor, NY: Cold Spring Harbor Laboratory Press; 2001.
20. Furuyama K, Fujita H, Nagai T, et al. Pyridoxine refractory X-linked sideroblastic anemia caused by a point mutation in the erythroid 5-aminolevulinate synthase gene. Blood. 1997;90:822–830.
21. Furuyama K, Harigae H, Heller T, et al. Arg452 substitution of the erythroid-specific 5-aminolaevulinate synthase, a hot spot mutation in X-linked sideroblastic anaemia, does not itself affect enzyme activity. Eur J Haematol. 2006;76:33–41.
22. Furuyama K, Sassa S. Interaction between succinyl CoA synthetase and the heme-biosynthetic enzyme ALAS-E is disrupted in sideroblastic anemia. J Clin Invest. 2000;105:757–764.
23. Kaneko K, Furuyama K, Aburatani H, Shibahara S. Hypoxia induces erythroid-specific 5-aminolevulinate synthase expression in human erythroid cells through transforming growth factor-beta signaling. FEBS J. 2009;276:1370–1382.
24. Guernsey DL, Jiang H, Campagna DR, et al. Mutations in mitochondrial carrier family gene SLC25A38 cause nonsyndromic autosomal recessive congenital sideroblastic anemia. Nat Genet. 2009;41:651–653.
25. Ye H, Jeong SY, Ghosh MC, et al. Glutaredoxin 5 deficiency causes sideroblastic anemia by specifically impairing heme biosynthesis and depleting cytosolic iron in human erythroblasts. J Clin Invest. 2010;120:1749–1761.
26. Allikmets R, Raskind WH, Hutchinson A, Schueck ND, Dean M, Koeller DM. Mutation of a putative mitochondrial iron transporter gene (ABC7) in X-linked sideroblastic anemia and ataxia (XLSA/A). Hum Mol Genet. 1999;8:743–749.
27. Bykhovskaya Y, Casas K, Mengesha E, Inbal A, Fischel-Ghodsian N. Missense mutation in pseudouridine synthase 1 (PUS1) causes mitochondrial myopathy and sideroblastic anemia (MLASA). Am J Hum Genet. 2004;74:1303–1308.
28. Ricketts CJ, Minton JA, Samuel J, et al. Thiamine-responsive megaloblastic anaemia syndrome: long-term follow-up and mutation analysis of seven families. Acta Paediatr. 2006;95:99–104.
29. Rotig A, Colonna M, Bonnefont JP, et al. Mitochondrial DNA deletion in Pearson's marrow/pancreas syndrome. Lancet. 1989;1:902–903.
30. Bergmann AK, Campagna DR, McLoughlin EM, et al. Systematic molecular genetic analysis of congenital sideroblastic anemia: evidence for genetic heterogeneity and identification of novel mutations. Pediatr Blood Cancer. 2010;54:273–278.
31. Cotter PD, Rucknagel DL, Bishop DF. X-linked sideroblastic anemia: identification of the mutation in the erythroid-specific delta-aminolevulinate synthase gene (ALAS2) in the original family described by Cooley. Blood. 1994;84:3915–3924.
32. Cotter PD, May A, Fitzsimons EJ, et al. Late-onset X-linked sideroblastic anemia. Missense mutations in the erythroid delta-aminolevulinate synthase (ALAS2) gene in two pyridoxine-responsive patients initially diagnosed with acquired refractory anemia and ringed sideroblasts. J Clin Invest. 1995;96:2090–2096.
33. Prades E, Chambon C, Dailey TA, Dailey HA, Briere J, Grandchamp B. A new mutation of the ALAS2 gene in a large family with X-linked sideroblastic anemia. Hum Genet. 1995;95:424–428.
34. Furuyama K, Uno R, Urabe A, et al. R411C mutation of the ALAS2 gene encodes a pyridoxine-responsive enzyme with low activity. Br J Haematol. 1998;103:839–841.
35. Harigae H, Furuyama K, Kudo K, et al. A novel mutation of the erythroid-specific delta-Aminolevulinate synthase gene in a patient with non-inherited pyridoxine-responsive sideroblastic anemia. Am J Hematol. 1999;62:112–114.
36. Furuyama K, Harigae H, Kinoshita C, et al. Late-onset X-linked sideroblastic anemia following hemodialysis. Blood. 2003;101: 4623–4624.
37. Ferreira GC, Neame PJ, Dailey HA. Heme biosynthesis in mammalian systems: evidence of a Schiff base linkage between the pyridoxal 5'-phosphate cofactor and a lysine residue in 5-aminolevulinate synthase. Protein Sci. 1993;2:1959–1965.
38. Gong J, Ferreira GC. Aminolevulinate synthase: functionally important residues at a glycine loop, a putative pyridoxal phosphate cofactor-binding site. Biochemistry. 1995;34:1678–1685.
39. Tan D, Ferreira GC. Active site of 5-aminolevulinate synthase resides at the subunit interface. Evidence from in vivo heterodimer formation. Biochemistry. 1996;35:8934–8941.
40. Gong J, Hunter GA, Ferreira GC. Aspartate-279 in aminolevulinate synthase affects enzyme catalysis through enhancing the function of the pyridoxal 5'-phosphate cofactor. Biochemistry. 1998;37:3509–3517.
41. Tan D, Barber MJ, Ferreira GC. The role of tyrosine 121 in cofactor binding of 5-aminolevulinate synthase. Protein Sci. 1998;7:1208–1213.

42. Tan D, Harrison T, Hunter GA, Ferreira GC. Role of arginine 439 in substrate binding of 5-aminolevulinate synthase. Biochemistry. 1998; 37:1478–1484.
43. Turbeville TD, Zhang J, Hunter GA, Ferreira GC. Histidine 282 in 5-aminolevulinate synthase affects substrate binding and catalysis. Biochemistry. 2007;46:5972–5981.
44. Lendrihas T, Zhang J, Hunter GA, Ferreira GC. Arg-85 and Thr-430 in murine 5-aminolevulinate synthase coordinate acyl-CoA-binding and contribute to substrate specificity. Protein Sci. 2009;18:1847–1859.
45. Lendrihas T, Hunter GA, Ferreira GC. Serine 254 enhances an induced fit mechanism in murine 5-aminolevulinate synthase. J Biol Chem. 2010;285:3351–3359.
46. Lendrihas T, Hunter GA, Ferreira GC. Targeting the active site gate to yield hyperactive variants of 5-aminolevulinate synthase. J Biol Chem. 2010;285:13704–13711.
47. Zhang J, Ferreira GC. Transient state kinetic investigation of 5-aminolevulinate synthase reaction mechanism. J Biol Chem. 2002;277: 44660–44669.

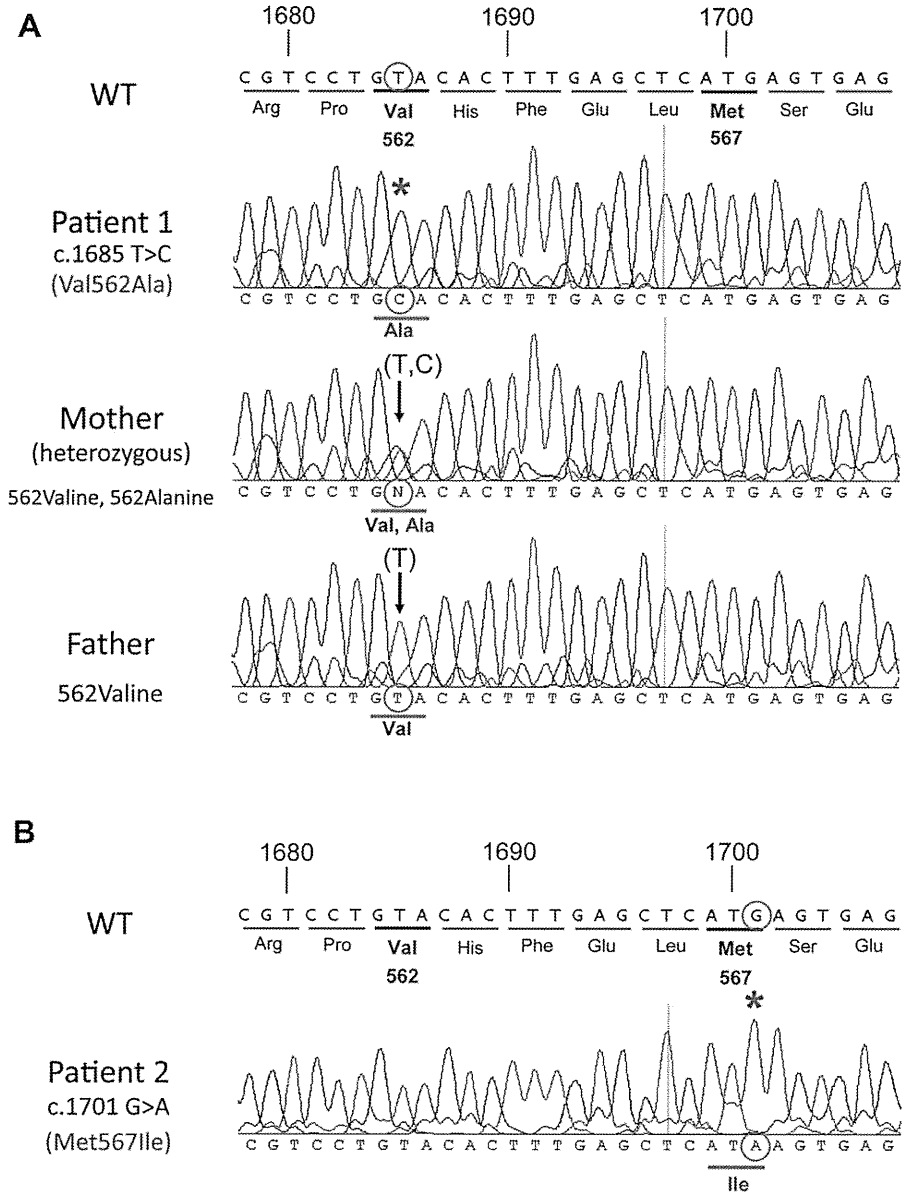

Supplementary Figure E1. Direct sequencing of 11th exon of ALAS2 gene in patients with sideroblastic anemia. Exon 11 of ALAS2 gene from each proband was amplified by PCR, and the amplicon was sequenced directly. Numbers shown at top indicate the positions of cDNA sequence, which is started from the first nucleotide of the ATG-translation initiation codon. Second and third lines indicate wild-type DNA sequence and amino acid sequence, respectively. Identified mutations are indicated with asterisks, and the expected amino acid substitution is shown under each mutation. (**A**) The c.1685T > C mutation of ALAS2 gene in case 1. The heterozygous condition of proband's mother and the wild-type allele of proband's father are shown. (**B**) The c.1701G > A mutation of ALAS2 gene in case 2.

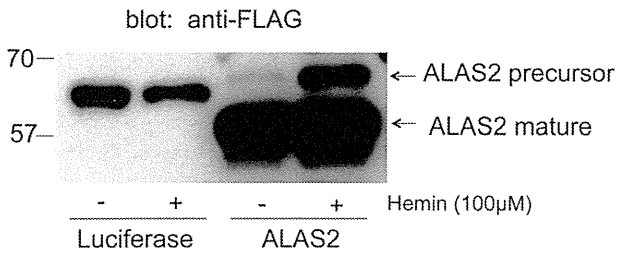

Supplementary Figure E2. Transient expression of FLAG-ALAS2 and FLAG-Luciferase in HeLa cells. HeLa human cervical cancer cells were transfected with FLAG-ALAS2 or FLAG-luciferase expression vector, then treated with 100 μM hemin. Cell lysates were subjected to the Western blot analysis with anti-FLAG antibody. Shown are the representative data.

Process for immune defect and chromosomal translocation during early thymocyte development lacking ATM

Takeshi Isoda,[1] Masatoshi Takagi,[1] Jinhua Piao,[1] Shun Nakagama,[1] Masaki Sato,[1] Kyoko Masuda,[2] Tomokatsu Ikawa,[2] Miyuki Azuma,[3] Tomohiro Morio,[1] Hiroshi Kawamoto,[2] and Shuki Mizutani[1]

[1]Department of Pediatrics and Developmental Biology, Graduate School of Medicine, Tokyo Medical and Dental University, Tokyo, Japan; [2]Laboratory for Lymphocyte Development, RIKEN Research Centre for Allergy and Immunology, Tokyo, Japan; and [3]Department of Molecular Immunology, Tokyo Medical and Dental University, Tokyo, Japan

Immune defect in ataxia telangiectasia patients has been attributed to either the failure of V(D)J recombination or class-switch recombination, and the chromosomal translocation in their lymphoma often involves the TCR gene. The ATM-deficient mouse exhibits fewer CD4 and CD8 single-positive T cells because of a failure to develop from the CD4$^+$CD8$^+$ double-positive phase to the single-positive phase. Although the occurrence of chromosome 14 translocations involving TCR-δ gene in ATM-deficient lymphomas suggests that these are early events in T-cell development, a thorough analysis focusing on early T-cell development has never been performed. Here we demonstrate that ATM-deficient mouse thymocytes are perturbed in passing through the β- or γδ-selection checkpoint, leading in part to the developmental failure of T cells. Detailed karyotype analysis using the in vitro thymocyte development system revealed that RAG-mediated TCR-α/δ locus breaks occur and are left unrepaired during the troublesome β- or γδ-selection checkpoints. By getting through these selection checkpoints, some of the clones with random or nonrandom chromosomal translocations involving TCR-α/δ locus are selected and accumulate. Thus, our study visualized the first step of multistep evolutions toward lymphomagenesis in ATM-deficient thymocytes associated with T-lymphopenia and immunodeficiency. (*Blood.* 2012;120(4):789-799)

Introduction

Ataxia telangiectasia (AT) is an autosomal recessive disorder that is characterized by cerebellar ataxia, telangiectasia, immune defects, and a predisposition to malignancy, particularly leukemia/lymphoma.[1-4] The immune defects observed in AT patients include fewer than normal T and B lymphocytes and lower serum IgA, IgG2, and IgE levels.[5,6] The ATM knockout (ATM$^{-/-}$) mouse has fewer CD4 and CD8 single-positive (SP) T cells because of a failure to develop from the CD4$^+$CD8$^+$ double-positive (DP) phase to the SP phase has been noted.[7-9]

The responsible gene ATM works as a master regulator for maintaining DNA integrity and has crucial role for responding DNA double-strand break (DSB) from extrinsic and intrinsic factors, such as ionizing radiation, free oxygen radicals, unscheduled replicative stimuli, and DSB during V(D)J recombination.[1-4,10] The role of ATM for V(D)J recombination of lymphocyte antigen receptor gene assembly or immunoglobulin synthesis is relatively well characterized. V(D)J recombination is initiated by the recombination activating genes (RAG)1 and RAG2 endonuclease. RAG protein binds and cleaves the DNA at specific recombination signal sequences (RSSs) that flank each V, D, and J gene segment.[11] After cleavage, ATM and other DNA damage response proteins, such as NBS1, 53BP1, and phosphorylated H2AX localize to DSBs.[12] Concurrently, classic nonhomologous end-joining complex is recruited.[13] Recruitment of these molecules functions directly in the repair of chromosomal DNA DSBs by maintaining DNA ends in repair complexes. These processes promote correct resolution of inversional V(D)J recombination and prevent aberrant antigen receptor locus translocations.[14] ATM deficiency leads to inefficient coding end binding after the RAG-dependent DSB generation at immunoglobulin and T-cell antigen receptor loci.[15] Transition failure from DP to SP observed in ATM$^{-/-}$ mice has been explained because of decreased efficiency in V-J rearrangement of the T-cell receptor (*Tcr*) α locus, accompanied by increased frequency of unresolved *TcrJα* coding end breaks.[8,9]

Most of thymic lymphomas observed in ATM knockout mouse recapitulate these aspects of human AT and possess chromosome 14 translocations at the *Tcrα/δ* locus preferentially with chromosome 12 where mouse *BCL11b* gene located, and mostly express CD4$^+$CD8$^+$ phenotype.[7,16] Interestingly, recent finding revealed that recurrent chromosome 14 translocations observed in ATM-deficient thymic lymphomas are associated with V(D)J recombination errors at *Tcrδ*, as opposed to *Tcrα* locus. In addition, *Eα* is completely dispensable for the oncogenic processes leading to these tumors.[17]

During T-cell development, early T-cell precursors differentiate first into CD4$^-$CD8$^-$ double-negative (DN) and then to DP stages. CD4$^-$CD8$^-$ DN T-cell subsets are further subdivided into DN1 to DN4 based on their expression of CD25 and CD117.[18] Rearrangement of TCR-β, -γ, and -δ genes occurs mainly at the DN3 stage, although TCR-δ and -γ genes are thought to be partially rearranged at DN1 and DN2 stages. Successful rearrangement of TCR genes in DN3 cells drives their further differentiation. DN3 stage is subdivided into DN3a and DN3b depending on the successful TCR-β rearrangement, which is followed by the DN4 stage.[19]

Submitted February 26, 2012; accepted June 6, 2012. Prepublished online as *Blood* First Edition paper, June 18, 2012; DOI 10.1182/blood-2012-02-413195.

The online version of this article contains a data supplement.

The publication costs of this article were defrayed in part by page charge payment. Therefore, and solely to indicate this fact, this article is hereby marked "advertisement" in accordance with 18 USC section 1734.

It has been speculated that immunodeficiency and susceptibility to lymphoma in AT are the result of a defective TCR recombination and/or class switch recombination. Although the chromosome 14 translocations involving the breaks at TCR-δ locus in ATM-deficient T cells suggest these to be early events in T-cell development, in-depth analyses focusing on early T-cell development at DN phase has not been elucidated. Here we show that ATM-deficient thymocytes fail to progress from DN3a to DN3b, and chromosome 14 breaks and translocations involving TCR-α/δ locus concurrently occur during this transitional stage.

Methods

Mice

$ATM^{+/-}$ mice, originally on the129SvJ × C57BL/6 background, were a kind gift from Dr P. J. McKinnon (St Jude Children's Research Hospital, Memphis, TN).[20] The $ATM^{+/-}$ mice were backcrossed for more than 15 generations with C57BL/6 mice. $ATM^{+/+}$ and $ATM^{-/-}$ mice were analyzed at 6 to 10 weeks of age. The *Atm* genotype was confirmed by PCR using tail DNA. $RAG2^{-/-}$ mice (BALB/c) and congenic CD45.1 mice (C57BL/6) were obtained from The Jackson Laboratory. The $RAG2^{-/-}$ mice were backcrossed with C57BL/6 mice. To generate mice deficient for both RAG2 and ATM, $RAG2^{-/-}$ and $ATM^{+/-}$ mice were crossed and the progeny were typed by PCR. All of the mice were bred in the specific pathogen-free unit in the vivarium in Tokyo Medical and Dental University. Animal care was approved by the Animal Care and Use Committee (protocol no. 0120228B). Sterile anti-CD3ε mAb (145-2C11) was injected intraperitoneally (150 μg/mouse).

Antibodies, flow cytometry, sorting, intracellular staining, and apoptosis analysis

Samples from thymi or cultured cells were stained using 5 or 6 antibody color combinations. The data were acquired on a FACSCalibur or FACSAria II (BD Biosciences) flow cytometry and analyzed using CellQuest Version 3.3 or FACSDIVA software. Each differential thymocyte phase was sorted by FACSAria II Version 6.1.3 (BD Biosciences) with more than 99% purity. The following antibodies were purchased from BD Biosciences: anti–mouse CD3ε NA/LE, PE/Cy7 (145-2C11), CD25 PE, PE/Cy7 (PC61), CD27 PE (LG.3A10), CD44 APC (IM7), CD45 PE/Cy5, PE/Cy7 (30-F11), CD117 APC (2B8), γδ T-cell receptor PE (GL3), TCR-β chain FITC (H57-597), 7-amino-actinomycin D, annexin V, CD3 molecular complex FITC (17A2), CD4 FITC (RM4-5), CD8a FITC, PE (53-6.7), CD11b FITC (M1/70), TER-119 FITC (TER-119), Gr-1 FITC (RB6-8C5), CD19 FITC (1D3), B220 FITC (RA3-6B2), and NK1.1 FITC (PK136). The following antibodies were purchased from BioLegend: CD27 PerCP/Cy5.5 (LG.3A10), CD45.1 PE/Cy7 (A20), CD45.2 APC/Cy7, (104) CD117 APC/Cy7 (2B8), γδ T-cell receptor APC (GL3), TCR-β chain PerCP/Cy5.5, and APC-Cy7 (H57-597). The phospho-histone H2A.X (Ser139) Alexa-647 (20E3) antibody was purchased from Cell Signaling. The following were used as lineage markers: CD3, CD4, CD8, CD19, B220, $CD11b^{-}$, Gr1, NK1.1, and TER119. We measured intracellular TCR-β, TCR-γδ and pH2AX by flow cytometry using the IntraPrep Kit (Beckman Coulter). For apoptosis analysis, the cells were stained with the surface marker for 15 minutes, washed in 1% BSA containing PBS, and then stained with annexin V and 7-amino-actinomycin D in annexin V binding buffer according to the manufacturer's instructions (BD Biosciences).

Cell-cycle analysis

We used Click-iT EdU flow cytometry assay kits for cell-cycle analysis (Invitrogen). The mice were injected intraperitoneally with 100 μg of EdU in PBS. After 3 hours, single-cell suspensions were prepared from thymi and stained for cell surface markers. DN2, DN3a, DN3b, and DP stage thymocytes were all sorted by FACSAria II. The sorted cells were subjected to EdU detection according to the protocol of the manufacturer and analyzed with the FACSCalibur.

PCR detection for TCR-β V(D)J and DJ rearrangement

TCR gene rearrangement was analyzed as previously described.[21] Genomic DNA was extracted from each thymocyte differentiation stage using a QIAamp DNA blood mini-kit (QIAGEN). The reaction volume was 25 μL and contained 10 ng of genomic DNA, 2.5 μL of 10× PCR buffer, 4 μL of 2.5mM dNTPs, 2.5 μL of 25μM $MgCl_2$, 0.4μM of each primer, and 2.5 U of LA Taq polymerase (TaKaRa Biotechnology). The PCR reactions were performed as follows: 5 minutes at 95°C followed by 33 to 35 cycles of 30 seconds at 95°C, 30 seconds at 60°C, and 2 minutes at 68°C, and a final extension for 7 minutes at 72°C with the GeneAmp PCR System 9700 (Applied Biosystems). The PCR products were analyzed on agarose gels stained with ethidium bromide.

Real-time PCR

Total RNA was isolated from DN2, DN3a, DN3b, DN4, and DP cells using an RNeasy kit (QIAGEN). cDNA was synthesized using Superscript III (Invitrogen) according to the protocol of the manufacturer. Real-time PCR was performed using SYBR Green, and the reactions were monitored using a LightCycler 480 (Roche Diagnostics). The reactions were performed in duplicate at 95°C for 5 minutes for denaturation followed by 40 cycles of 95°C for 10 seconds, 60°C for 10 seconds, and 72°C for 10 seconds. The primer sequences used are those described previously for pre–TCR-α,[22] BCL11b,[23] RAG1, and RAG2.[24]

Growth factors

Recombinant murine stem cell factor, recombinant murine FMS-like tyrosine kinase ligand (Flt3L), and rmIL-7 were purchased from R&D Systems.

Isolation of adult long-term repopulating hematopoietic stem cells

Single-cell suspensions of BM cells were prepared from 4- to 8-week-old mice. The cells were incubated with anti-Sca1 and anti-CD105 mAbs for 15 minutes on ice. Next, MACS magnetic beads were used for $Sca1^{+}$ and $CD105^{+}$ enrichment in a 2-step process according to the protocol of the manufacturer (Miltenyi Biotec).

In vitro differentiation of long-term repopulating hematopoietic stem cells

We cultured OP9-DLL1 cells in a 10-cm or 6-well plate with α-MEM medium containing 20% FBS, streptomycin (100 mg/mL), and penicillin (100 U/mL) at 37°C in a humidified atmosphere containing 5% CO_2. Approximately 1 to 3 × 10^4 long-term repopulating hematopoietic stem cells per well were cultured on semiconfluent OP9-DLL1 cells in medium containing 5 ng/mL of Flt3L and 1 ng/mL of IL-7. Floating cells were transferred to a fresh monolayer of semiconfluent OP9-DLL1 cells on days 6, 10, 14, and 18. For *N*-acetyl-*L*-cysteine (NAC) experiments, the cells were incubated with 100μM or1mM NAC (Sigma-Aldrich). Singly sorted DN3a and DN3b cells from WT and $ATM^{-/-}$ thyme were cultured on OP9-DLL1 cells containing 5 ng/mL Flt3L and 1 ng/mL IL-7 in 96-well plates.

Bone marrow transplantation

Recipient mice (CD45.1) received myeloablative conditioning with 10 Gy of total body irradiation 6 hours before bone marrow transplantation (BMT). Bone marrow cells were harvested from donor mice (CD45.2) on the day of BMT and injected (1 × 10^7cells) into the tail vein of recipient mice. The mice received ad libitum drinking water containing 1 mg/mL neomycin trisulphate salt hydrate (Sigma-Aldrich) and 100 U/mL polymyxin B sulfate salt (Sigma-Aldrich).

FISH analysis of chromosome 12, chromosome 14, and the TCR-α/δ locus in DN phase thymocytes

To obtain DN2/DN3a cells, long-term repopulating hematopoietic stem cells were cultured on OP9-DLL1 cells in α-MEM containing 20% FBS, streptomycin (100 mg/mL), penicillin (100 U/mL), and 10 ng/mL of Flt3L, IL-7, and stem cell factor. To generate metaphase spreads, day 15 to 17 DN2/DN3a cells were treated with 25 ng/mL colcemid (Sigma-Aldrich) for 2 hours. To collect DN3b/DN4 cells, we continued to cultivate differentiated DN2/DN3a cells in the same medium, but containing 5 ng/mL Flt3L and 1 ng/mL IL-7 for 7 to 10 additional days. After 25 ng/mL colcemid treatment for 2 hours, the DN3b/DN4 cells were sorted using a FACSAria II. DN2/DN3a cells and DN3b/DN4 cells were treated in hypotonic solution containing 0.06M potassium chloride and 0.02% sodium citrate solution for 20 minutes and then fixed in methanol and acetic acid. To perform FISH assays for the TCR-α/δ locus breaks, we used BAC probes for the 5′-end (RP23-204N18; 5′; blue) and 3′-end (RP23-10K20; green) of the TCR-α/δ locus. The BACs were labeled by amine-nick translation using the FISH Tag DNA multicolor kit according to the manufacturer's protocol (Invitrogen). Chromosome 12 (green) and 14 (red) paint probes were purchased from Applied Spectral Imaging. The painting probes (10 μL) were mixed with 100 ng of 5′- and 3′-TCR α/δ locus probes and denatured at 80°C for 10 minutes before use. The slides were denatured at 67°C for 90 seconds and dehydrated in a cold ethanol series of 70%, 90%, and 100%. Hybridization was performed for 20 hours in a humidified chamber at 37°C. The slides were stringently washed in 0.4 × saline sodium citrate at 73°C for 4.5 minutes followed by 4 × saline sodium citrate/0.1% Tween-20 for 2 minutes and then mounted in SlowFade Gold antifade reagent (Invitrogen) with 4,6-diamidino-2-phenylindole (Vector Laboratories). Images were captured with an FV10i confocal microscope (Olympus). Image acquisition and processing were performed using an Olympus FluoView Version 3.0 Viewer (Olympus).

Data analysis

Data are expressed as mean plus or minus SE. Unpaired *t* tests or ANOVA were used for statistical analysis. *P* values less than .05 were considered significant.

Results

Impaired development from DN3a to DN3b in ATM $^{-/-}$ thymus in vivo

Consistent with previous reports,[8,9] the proportion of CD4SP and CD8SP cells was decreased (Figure 1A) and total thymocyte numbers were significantly reduced in ATM$^{-/-}$ mice (Figure 1B). The relative percentage of cells in the DN phase was significantly higher in ATM$^{-/-}$ than in ATM$^{+/+}$ mice (Figure 1C); and although the relative percentage of cells in DN1 and DN2 was slightly lower in total thymocytes of ATM knockout mice, there was an accumulation of cells in DN3 (Figure 1D-E). Interestingly, DN3b cells, which are characterized by the expression of CD27 and intracellular TCR-β or TCR-γδ, were significantly reduced in ATM$^{-/-}$ mice (Figure 1F-I). Collectively, these data indicate that ATM-deficient thymocytes fail to transit from the DN3a to the DN3b stage in both γδ T-cell and αβ T-cell lineages in vivo.

Transition failure from DN3a to DN3b of ATM$^{-/-}$ thymocyte in vitro

To further evaluate the failure in transition from DN3a to DN3b, we took advantage of an in vitro thymocyte development system. CD105^{+}Sca-1^{+} BM cells, which represent a progenitor population containing hematopoietic stem cells (hereafter referred to as BM progenitors), from ATM$^{+/+}$ and ATM$^{-/-}$ mice were cocultured on OP9-Delta like 1 (DLL1) cells with Flt3L and IL-7.[25] DP cells began to appear on day 10 in ATM$^{+/+}$ cell cultures and gradually accumulated. By contrast, DP cell production was not seen until day 14 in the ATM$^{-/-}$ cultures (Figure 2A-B). The DN phase profile gated on a lineage-negative fraction showed a failure in transition from DN3 to DN4 for the ATM$^{-/-}$ BM progenitors (Figure 2C-D). Analysis of intracellular (ic) TCR-β expression in the ATM$^{-/-}$ DN3 population allowed us to focus on the defect in the transition from the DN3a to the DN3b stage (Figure 2E-F). Neither T-cell development nor the transition from DN3a to DN3b in ATM$^{-/-}$ BM progenitors was restored by the treatment with 100μM or 1mM antioxidant NAC (supplemental Figures 1-3, available on the *Blood* Web site; see the Supplemental Materials link at the top of the online article), ruling out the possibility that oxidative stress is involved in these processes, which was in contrast to the previous findings in the maintenance of HSCs and T-cell development.[26,27] To directly demonstrate that the developmental failure of T cells in ATM$^{-/-}$ lies in the transition from DN3a to DN3b, singly sorted DN3a and DN3b cells of wild-type and knockout mice were cultured on OP9-DLL1 and analyzed for their potential to differentiate into DP cells. These clonal assays also confirmed that the DN3a stage cells fail to transit to DP cells in ATM$^{-/-}$ cells (10% ± 0.78% frequency) compared with ATM$^{+/+}$ cells (34.2% ± 4.59% frequency). However, ATM$^{-/-}$ DN3b cells differentiated into DP cells as efficiently as the ATM$^{+/+}$ cells (Figure 2G). Thus, the in vivo transitional failure from DN3a to DN3b was recapitulated in an in vitro system.

Inefficient TCR-γδ lineage differentiation in ATM$^{-/-}$ mice

The ratio of peripheral TCR-γδ to TCR-αβ T cells (TCR-γδ/TCR-αβ) in AT patients is reportedly relatively higher.[28] Consistent with previous reports, the TCR-γδ cell population was relatively higher in ATM$^{-/-}$ mice thymus (Figure 3A). However, the absolute number of TCR-β and TCR-γδ–positive cells was significantly decreased in ATM$^{-/-}$ thymus than ATM$^{+/+}$ thymus (Figure 3B). Then, in vitro T-cell differentiation system using BM progenitors was used to determine how cell surface TCR-β and γδ expression is deregulated in ATM$^{-/-}$ cells, as reflected by the delay or decrease in numbers of TCR-γδ and TCR-β T cells (Figure 3C-D). Possible involvement of reactive oxygen species was evaluated by NAC treatment, and NAC was shown not to improve the failure of TCR-β and TCR-γδ expression in ATM$^{-/-}$ thymocytes (supplemental Figure 4A-B). Thus, γδ-TCR lineage development is also affected in ATM$^{-/-}$ mice, but this was not reactive oxygen species dependent.

ATM is not involved in differentiation program from DN3 to DP

To confirm that the developmental program occurring from DN3b to DP stages is intact, we examined T-cell development in RAG2$^{-/-}$ mice. In both ATM$^{+/+}$RAG2$^{-/-}$ and ATM$^{-/-}$RAG2$^{-/-}$ mice, thymocytes accumulated equally at the DN3 stage, indicating that ATM has no effect on the development up to the β-selection checkpoint (supplemental Figure 5A), which is the gatekeeper for cells with a functional TCR-β chain. The developmental arrest at DN3 in RAG2$^{-/-}$ mice can be bypassed by stimulation of the pre-TCR complex (TCR-β/pTα/CD3) with anti-CD3ε antibody, allowing one to analyze the integrity of this signaling pathway in cell differentiation.[29] By anti-CD3ε stimulation, thymocytes from ATM$^{-/-}$RAG2$^{-/-}$ mice arrested at the DN3 stage differentiated into the DP stage as efficiently as those from ATM$^{+/+}$RAG2$^{-/-}$ mice, and there was no difference in cell expansion efficiency